Word Count: 4568

Revision 2

Single-crystal Elasticity of Humite-Group Minerals by Brillouin Scattering

QINGCHUN ZHANG[1], XINYUE ZHANG[1], LUO LI[1], ZHU MAO[1,2,3,*], XIANG WU[4]

[1]Deep Space Exploration Laboratory / School of Earth and Space Sciences, University of Science and Technology of China, Hefei 230026, China

[2]CAS Center for Excellence in Comparative Planetology, University of Science and Technology of China, Hefei, Anhui 230026, China

[3]Frontiers Science Center for Planetary Exploration and Emerging Technologies, University of Science and Technology of China, Hefei, Anhui 230026, China

[4]State Key Laboratory of Geological Processes and Mineral Resources, China University of Geosciences, Wuhan 430074, China

*Corresponding authors: Zhu Mao (zhumao@ustc.edu.cn)

ABSTRACT

Humite-group minerals play a crucial role in transporting water and fluorine to the Earth's deep mantle through slab sinking. In this study, we have used Brillouin scattering to determine the single-crystal elastic constants of four natural humite-group minerals with varying H_2O and fluorite contents under ambient conditions, including one chondrodite [$Mg_{4.88}Si_{1.94}O_8(OH_{0.78}F_{1.22})$] ($F_{61}$-Chn), one humite [$Mg_{7.03}Si_{3.07}O_{12}(OH_{1.26}F_{0.74})$] ($F_{37}$-Hu), and two clinohumite [$Mg_{8.85}Ti_{0.19}Si_{3.93}O_{16}(OH_{1.11}F_{0.89})$ and $Mg_{8.63}Fe_{0.10}Ti_{0.24}Si_{3.97}O_{16}(OH_{1.84}F_{0.16})$] ($F_{45}$-Chu and F_8-Chu) samples. The adiabatic bulk (K_{S0}) and shear (G_0) moduli calculated from the elastic constants using Voigt-Reuss-Hill averages are: K_{S0} = 120.4(3) GPa and G_0 = 74.1(5) GPa for F_{61}-Chn, K_{S0} = 122.4(3) GPa and G_0 = 78.4(2) GPa for F_{37}-Hu, K_{S0} = 126.2(3) GPa and G_0 = 79.7(2) GPa for F_{45}-Chu, and K_{S0} = 120.5(3) GPa and G_0 = 76.8(2) GPa for F_8-Chu. Our results indicate that the addition of F leads to a noticeable increase in the elasticity of clinohumite and chondrodite, which is in contrast to the effect of H_2O. Although Fe has a negligible effect on the bulk modulus of clinohumite, it can produce a substantial decrease in the shear modulus. These results provide important insights into the influence of humite-group minerals on the mantle velocity structure. Furthermore, we have investigated the influence of composition on the elasticity and sound velocities of minerals along the forsterite-brucite join in the MgO-SiO_2-H_2O system, confirming previous observations. Increasing H_2O content along the forsterite-brucite join leads to apparent reductions in the elasticity and sound velocities. The influence of Fe on the elasticity and sound velocities of these minerals has also been evaluated.

Keywords: clinohumite, humite, chondrodite, single-crystal elasticity, Brillouin spectroscopy

This is the peer-reviewed, final accepted version for American Mineralogist, published by the Mineralogical Society of America.
The published version is subject to change. Cite as Authors (Year) Title. American Mineralogist, in press.
DOI: https://doi.org/10.2138/am-2023-9067. http://www.minsocam.org/

INTRODUCTION

Subduction is a crucial process in redistributing volatile elements between the Earth's surface and interior. Despite the fact that most volatiles return to the surface at relatively shallow depths during slab sinking, some minerals, including serpentine, lawsonite, aragonite, and magnesite, are capable of transporting water and carbon into the deeper mantle (Dasgupta and Hirschmann, 2010; Dixon et al., 2002; Flemetakis et al., 2022; Kaminsky, 2012; Kobayashi et al., 2017; Ohtani et al., 2018; Thompson, 1992; Wirth et al., 2009). Among volatile-rich minerals, the humite-group minerals [$nM_2SiO_4 \cdot M_{1-x}Ti_x(F, OH)_{2-2x}O_{2x}$] have long been considered as significant water and fluorine carriers in subduction slabs (Figure 1) (Akimoto et al., 1977; Engi and Lindsley, 1980; Rice, 1980). Here, M denotes Mg with minor amounts ($x < 0.5$) of Fe, Mn, Ca, etc., and n equals 1, 2, 3, and 4, representing norbergite, chondrodite, humite, and clinohumite, respectively. These minerals naturally form as the product of metamorphism (associated with granitic intrusions) (Evans and Trommsdorff, 1983; Hermann et al., 2007; Selyatitskii and Reverdatto, 2022; Shen et al., 2015). The similarity of the ionic radii of fluorine and hydroxyl (~1.33 Å and 1.40 Å, respectively) with the equal charge allows for the substitution of OH by F in the structure of humite-group minerals (Hughes and Pawley, 2019). In nature, the fluorine concentration (X_F = F/(F+OH)) of these minerals ranges from 0.05 to 0.78 (Ehlers and Hoinkes, 1987).

Previous researches have shown that the high-pressure stability of OH-endmember humite-group minerals decreases with increasing temperature (Iwamori, 2004; Wunder, 1998; Yamamoto and Akimoto, 1977). Both OH-chondrodite and OH-clinohumite can only exist below ~950°C and ~1100°C at 12 GPa (~360-km depth), respectively (Burnley and Navrotsky, 1996; Komabayashi

et al., 2005; Smyth et al., 2006; Yamamoto and Akimoto, 1977). The stability of humite and norbergite has received less attention due to their low occurrence in rocks (Stalder and Ulmer, 2001). More importantly, the high-pressure stability of humite-group minerals is highly dependent on their fluorine (F) content (Grützner et al., 2017; Stalder and Ulmer, 2001). The addition of F can significantly broaden their stability field in the mantle (Grützner et al., 2017). In the MgO-SiO_2-F system, synthetic F-clinohumite, -humite, and -chondrodite can survive to temperatures above 1780 ℃ at 17 GPa, 200 ℃ higher than the normal upper mantle geotherm (Grützner et al., 2017).

The elastic properties of humite-group minerals are critical in determining seismic wave velocities and identifying their potential presence in the Earth's mantle. However, previous studies on the elasticity of clinohumite have shown complex compositional effects (Fritzel and Bass, 1997; Phan, 2008; Qin et al., 2017; Ross and Crichton, 2001). The isothermal bulk modulus of synthetic OH-clinohumite ($Mg_9Si_4O_{16}(OH)_2$), K_{T0}, is 119.4(7) GPa with a fixed $(\partial K_T/\partial P)_{T0}$ = 4.8(2), which is consistent with ultrasonic measurements with the adiabatic bulk modulus, K_{S0}, of 119(2) GPa (Phan, 2008; Ross and Crichton, 2001). This synthetic OH-clinohumite has a shear modulus, G_0, of 77(1) GPa (Phan, 2008). In comparison, Brillouin measurements have shown that the (Fe, F)-bearing clinohumite ($Mg_{8.16}Fe_{0.57}Si_4O_{16}(F_{0.57}, OH_{1.43})$) has a larger bulk modulus (K_{S0} = 125(2) GPa) and a smaller shear modulus (G_0 = 73(5) GPa) than the corresponding OH-bearing phase (Fritzel and Bass, 1997). However, these values are much smaller than the K_{T0} of 141-144 GPa for two natural (Ti, F)-bearing clinohumite derived from XRD measurements (Qin et al. (2017). Further research is needed to provide a comprehensive understanding of the influence of composition on the elasticity of clinohumite.

89

90 Similarly, K_{T0} of chondrodite also exhibits a strong dependence on the composition (Friedrich et
91 al., 2002). The K_{T0} of OH-chondrodite ($Mg_5Si_2O_8(OH)_2$) is 117(2)-118.4(2) GPa with a fixed
92 $(\partial K_T/\partial P)_{T0}$ = 4 from XRD measurements (Kuribayashi et al., 2004; Ross and Crichton, 2001).
93 Addition of Fe has a minor effect on the bulk modulus of OH-chondrodite. The adiabatic bulk
94 modulus (K_{S0}) of synthetic Fe-bearing OH-chondrodite ($Mg_{5.05}Fe_{0.06}Si_{1.95}O_8(OH)_2$) at ambient
95 conditions measured by Brillouin spectroscopy is 118(1) GPa, similar to the XRD results of the
96 corresponding Fe-free phase (Kuribayashi et al., 2004; Ross and Crichton, 2001). The combined
97 effect of Fe and F on the bulk modulus of chondrodite remains ambiguous. Although K_{T0} of (F,
98 OH)-chondrodite (X_F = 0.58-0.63) with 4.4-5.7 mol% Fe (X_{Fe} = Fe/(Ti+Fe+Mg)) are 122.0(3)-
99 124.1(4) GPa (Friedrich et al., 2002; Kuribayashi et al., 2004), Brillouin measurements on the
100 K_{S0} of (F, OH)-chondrodite with a similar Fe content of 5.4 mol% Fe and X_F = 0.32 yield a much
101 lower value of 118(2) GPa (Sinogeikin and Bass, 1999). And the shear modulus (G_0) of this Fe-
102 bearing (F, OH)-chondrodite is 75.6(7) GPa, which is greater than that of OH-chondrodite with
103 1.1 mol% Fe (G_0 = 70.6(5) GPa). The elasticity of humite and norbergite are rarely studied,
104 except Kuribayashi et al. (2008) reported the K_{T0} = 113(2) GPa of (F, OH)-norbergite
105 ($Mg_{2.98}Si_{0.99}O_4(F_{1.69}, OH_{0.31})$) using XRD. Further experimental investigation is thus needed to
106 better constrain the influence of composition and structure on the elasticity of humite-group
107 minerals.

108

109 In this study, we report the elasticity of four (F, OH)-humite group minerals using Brillouin
110 scattering at ambient conditions, including one chondrodite (Chon), one humite (Hu), and two
111 clinohumite (Chu) (Figure 2). We focus our attention on the compositional effects of the

elasticity of humite-group minerals, and by combining our results with all available data, we have further refined the previously established relationships for evaluating the correlation between H_2O content and elasticity for phases along the forsterite-brucite join in the MgO-SiO_2-H_2O system (Sanchez-Valle et al., 2006; Ye et al., 2015).

EXPERIMENTAL METHODS

Two clinohumite samples with a dark red color were from Morogoro, Tanzania, while the humite and chondrodite samples were from Mogok, Myanmar. All samples used in this study are natural gem-quality single crystals. The mineral compositions were determined by electron microprobe at the Key Laboratory of Crust-Mantle Materials and Environments, University of Science and Technology of China (USTC) (Table 1). Both clinohumite samples contain a certain amount of Ti with compositions of $Mg_{8.85}Ti_{0.19}Si_{3.93}O_{16}(OH_{1.11}F_{0.89})$ (F_{45}-Chu) and $Mg_{8.63}Fe_{0.10}Ti_{0.24}Si_{3.97}O_{16}(OH_{1.84}F_{0.16})$ (F_8-Chu). The humite and chondrodite samples display compositions of $Mg_{7.03}Si_{3.07}O_{12}(OH_{1.26}F_{0.74})$ (F_{37}-Hu) and $Mg_{4.88}Si_{1.94}O_8(OH_{0.78}F_{1.22})$ (F_{61}-Chn), respectively. Single-crystal X-ray diffraction was conducted to determine the sample lattice parameters using a Bruker D8 QUEST type X-ray diffractometer at the State Key Laboratory of Geological Processes and Mineral Resources, China University of Geosciences (Wuhan) (Table 2). The densities of the respective samples were calculated from the unit-cell volume together with the chemical formula (Table 2).

Each single crystal was cut into three platelets orthogonal to each other with random crystallographic orientations for Brillouin measurements. These platelets were double-side polished to a thickness of 40 μm, and then Brillouin spectroscopy experiments were performed

under ambient conditions. The Brillouin signals were excited by a 532-nm wavelength laser and captured using a six-pass Sandercock tandem Fabry-Perot interferometer (TFP-2 HC) equipped with a photodiode detector at the High-Pressure Mineral Physics Laboratory of the USTC (Lindsay et al., 1981; Sandercock, 1982). Further details of the Brillouin scattering system setup and the TFP interferometer can be found in references (Online Material[1] Figure S1) (Scarponi et al., 2017; Sinogeikin et al., 2006; Sinogeikin et al., 1998; Speziale et al., 2014). The external scattering angle was calibrated to be 49.5° by both using standard single-crystal MgO and BK-7 glass (Online Material[1] Table S1). When observed under a petrographic microscope and cross-polarized light, the double-side polished samples exhibit uniform interference colors, indicating the even thickness of our samples (Hou et al., 2022; Waters et al., 2021). Therefore, the impact of non-parallelism in the samples is negligible. In a symmetric forward scattering geometry, the measured Brillouin frequency shifts ($\Delta\nu_B$) were converted to the acoustic velocities (v) through the equation (Speziale et al., 2014; Whitfield et al., 1976):

$$v = \frac{\Delta\nu_B \lambda_0}{2\sin(\theta/2)} \quad (1)$$

where λ_0 is the laser wavelength (532 nm), and θ is the external scattering angle (49.5° in this study). Additionally, the Brillouin frequency shift corresponding to each channel number i of the spectrum is determined as follows (Zouboulis et al., 2014):

$$\Delta\upsilon = [-\frac{A}{\lambda_0} + (i-1)\times\frac{2A}{\lambda_0}]\times\frac{c}{N}\times \mathrm{FSR} \quad (2)$$

$$\mathrm{FSR} = \frac{1}{2nD} \quad (3)$$

where A is the scanning amplitude of the moving mirrors of the Fabry-Perot interferometer (580 nm in this experiment), c is the velocity of light in vacuum (3×10^8 m/s), N is the total number of

channels (it is set to 1024), FSR is the free spectral range of the interferometer, n is the refractive index (approximate to1), and D is the spacing between the two Fabry-Perot mirrors (0.7 cm, FP1). For each platelet, spectra were collected in 10° step over a range of 180°, with an average collection time of approximately 50 minutes per spectrum (Online Material[1] Tables S2-S5). The uncertainty in the measured velocities using Brillouin scattering in the diamond-anvil cell has been estimated to be less than 0.7% by considering statistical errors from individual peak fitting, the imperfect symmetry in the stocks and anti-stocks, slight misalignment between the two diamond anvils in the DAC, and weak angular deviations between the sample and the diamond culet (Sinogeikin and Bass, 2000; Zha et al., 1996). In most directions, we observed one quasi-longitudinal mode (V_P) and two quasi-shear modes (V_{S1} and V_{S2}). Representative Brillouin spectra are shown in Figure 3.

RESULTS

Clinohumite and chondrodite crystallize in the monoclinic system (*b*-unique, $P2_1/c$) and were characterized by 13 independent, non-zero elastic constants, while the orthorhombic humite (*Pmcn*) has 9 individual non-zero elastic constants. Single-crystal elastic constants, C_{ij}s, were derived from a least-squares fitting inversion of the Christoffel equation (Brown, 2018; Brown et al., 1989; Every, 1980):

$$\det\left|C_{ijkl}\, n_j\, n_l - \rho v^2 \delta_{ik}\right| = 0 \quad (4)$$

where C_{ijkl} is the elastic constant in the fourth rank tensor, n_j and n_l are the direction cosines of the phonon propagation directions, ρ is the density, v is the acoustic velocity from Brillouin measurements, and δ_{ik} is the Kronecker delta (Table 2). The crystallographic orientation for each platelet was identified by three Eulerian angles (θ, ψ, and χ), which relate the crystal reference to

the laboratory frame (Shimizu and Sasaki, 1992). To determine the elastic constants and Eulerian angles, we performed an iterative inversion process. We initially utilized existing C_{ij}s data from clinohumite and chondrodite samples (Fritzel and Bass, 1997; Sinogeikin and Bass, 1999), which share similar structures and compositions, as our initial input for orientation inversion. Following this, we constrained the orientation parameters and performed 2-3 times iterations to invert C_{ij}s. Subsequently, we simultaneously released constraints on both C_{ij}s and orientation and performed 2-3 times inversion iterations until the root mean square (RMS) remained unchanged, yielding the final result. Figures 4 and 5 present the variation of the measured acoustic velocities with respect to the azimuthal angles for each sample. Here, the RMS error for each fitting is less than 32 m/s (Table 3).

In the case of low-symmetry minerals like monoclinic clinohumite and chondrodite, selecting the appropriate combination of crystallographic orientations is crucial to accurately determine all the C_{ij}s. We conducted inversion sensitivity tests using velocities measured along 57 different crystallographic directions (Online Material[1] Figures S2-S3) and calculated correlation matrices (Online Material[1] Tables S6-S9). Our analysis demonstrates that all C_{ij}s of our humite-group samples can be well constrained by the measured sound velocities from three sample platelets. These results provide robust evidence for the accuracy and reliability of our modeled elastic moduli. We have also calculated the linear incompressibility, β, using the obtained single-crystal elastic moduli:

$$\beta = S_{ijkk} l_i l_j \tag{5}$$

where S_{ijkk} is elastic compliance constants, l_j and l_i are the unit vector. The matrix notation for the monoclinic and orthogonal crystal systems is represented by the following equations (Nye, 1957):

This is the peer-reviewed, final accepted version for American Mineralogist, published by the Mineralogical Society of America.
The published version is subject to change. Cite as Authors (Year) Title. American Mineralogist, in press.
DOI: https://doi.org/10.2138/am-2023-9067. http://www.minsocam.org/

Monoclinic system:

$$\beta = (S_{11}+S_{12}+S_{13})l_1^2 + (S_{12}+S_{22}+S_{23})l_2^2 + (S_{13}+S_{23}+S_{33})l_3^2 + (S_{15}+S_{25}+S_{35})l_3l_1 \quad (6)$$

Orthorhombic system:

$$\beta = (S_{11}+S_{12}+S_{13})l_1^2 + (S_{12}+S_{22}+S_{23})l_2^2 + (S_{13}+S_{23}+S_{33})l_3^2 \quad (7)$$

where $S_{ij} = C_{ij}^{-1}$. Therefore, for both monoclinic and orthorhombic crystals, the axial compressibility (β_a, β_b, and β_c) can be expressed as follows:

$$\begin{aligned} \beta_a &= S_{11}+S_{22}+S_{13} \\ \beta_b &= S_{12}+S_{22}+S_{23} \\ \beta_c &= S_{13}+S_{23}+S_{33} \end{aligned} \quad (8)$$

The corresponding axial compressibility of our experimental samples is listed in Table 3. Using the obtained single-crystal elasticity, we calculated the K_{S0} and G_0 via the Voigt-Reuss-Hill averaging scheme (Hill, 1963). The compressional wave velocity (V_P) and shear wave velocity (V_S) were calculated as follows:

$$V_P = \sqrt{\frac{K_{S0}+\frac{4}{3}G_0}{\rho}} \quad (9)$$

$$V_S = \sqrt{\frac{G_0}{\rho}} \quad (10)$$

The aggregate bulk and shear moduli for each sample are also shown in Table 3.

DISCUSSION

Clinohumite

Together with previous experimental results (Fritzel and Bass, 1997), we noted that all clinohumite samples display $C_{22}>C_{11}>C_{33}$ and $C_{66}\approx C_{44}>C_{55}$ (Table 3). In all the reported

This is the peer-reviewed, final accepted version for American Mineralogist, published by the Mineralogical Society of America.
The published version is subject to change. Cite as Authors (Year) Title. American Mineralogist, in press.
DOI: https://doi.org/10.2138/am-2023-9067. http://www.minsocam.org/

221 samples, a notable anisotropy in axial compressibility is observed, with $\beta_c > \beta_a > \beta_b$ (Table 3). This
222 indicates that clinohumite is most incompressible along the *b*-axis and has the lowest resistance
223 to shear in the (010) crystallographic plane. Previous X-ray diffraction experiments on natural
224 and synthetic clinohumite have also demonstrated the highest degree of linear incompressibility
225 along the *b*-axis, while the *c*-axis is most compressible (Qin et al., 2017; Ross and Crichton,
226 2001). It is known that the stiffness of a crystal is primarily controlled by the gross features of its
227 structure with composition playing a secondary role (Webb and Jackson, 1990). The zigzag
228 chains of edge-sharing MO_6-octahedra aligned along the *a*-axis which are cross-linked by SiO_4-
229 tetrahedra are the key crystal structural units of clinohumite (Figures 2a) (Ferraris et al., 2000;
230 Robinson et al., 1973). SiO_4-tetrahedra is more incompressible than MO_6-octahedra. SiO_4-
231 tetrahedron in clinohumite are connected by corner sharing along the *b*-axis, which may explain
232 the higher incompressibility of the *b*-axis than the other two axes (Bass et al., 1984; Sinogeikin
233 and Bass, 1999; Webb and Jackson, 1990).
234
235 Using the obtained elastic constants and density, we have calculated the velocity anisotropies of
236 clinohumite (Table 3). The azimuthal P-wave velocity anisotropy (AV_P) and S-wave splitting
237 (AV_S) are defined by (Karki et al., 2001):

238 $$AV_P = \frac{V_{P,max} - V_{P,min}}{V_{P,aver}} \times 100\% \quad (11)$$

239 $$AV_S = \frac{|V_{S1} - V_{S2}|}{V_{S,aver}} \times 100\% \quad (12)$$

240 where AV_S is the difference between the speeds of the two transverse polarizations (V_{S1} and V_{S2})
241 propagating in the same direction. The results reveal that the maximum AV_P of clinohumite is
242 parallel to the *b*-axis (polarization [010]), and the highest AV_S is present at ~45° between the *a*-

and *b*-axes. Together with previous experimental results, we have noted that clinohumite with varying F and Ti content has a similar AV_P value of 21.9-24.2% and AV_S of 15.0-16.5% (Table 3) (Fritzel and Bass, 1997). The single-crystal elastic anisotropy of clinohumite is similar to the upper-mantle olivine with AV_P = 25% and AV_S = 18% at ambient conditions (Jacobsen et al., 2008).

Using the obtained single-crystal elastic constants and density, we have computed the adiabatic bulk and shear moduli at ambient conditions and compared them with all available literature data derived from direct measurements by Brillouin scattering and ultrasonic study (Table 4) (Fritzel and Bass, 1997; Phan, 2008; Sinogeikin and Bass, 1999; Ye et al., 2015; Zhang et al., 2023). We first considered the influence of F and OH substitution on the elastic moduli of clinohumite. For clinohumite with Fe content less than 1.1 mol%, the substitution of OH by F leads to an obvious linear increase in the K_{S0} and G_0 following (the solid red lines in Figure 6a):

$$K_{S0} = 119.4(18) + 12.2(60) \times X_F \quad (13)$$

$$G_0 = 76.7(12) + 3.6(40) \times X_F \quad (14)$$

where X_F = F/(F+OH). Addition of Fe causes an apparent decrease in the G_0. Specifically, the G_0 of clinohumite with 6.1 mol% Fe and X_F = 0.29 is 7.1% lower than the corresponding Fe-free phase with the same F content. Due to limited experimental results for the elasticity and sound velocity of Fe-bearing humite-group minerals, it is challenging to accurately describe the combined effect of Fe and F (H_2O) on the elasticity and sound velocity of the humite-group minerals. We thus simply assume that the addition of Fe leads to a linear reduction in the elasticity and sound velocity of humite-group minerals for a given H_2O content. As a result, we

This is the peer-reviewed, final accepted version for American Mineralogist, published by the Mineralogical Society of America.
The published version is subject to change. Cite as Authors (Year) Title. American Mineralogist, in press.
DOI: https://doi.org/10.2138/am-2023-9067. http://www.minsocam.org/

provide a preliminary constraint on the combined effect of Fe and F on the G_0 of clinohumite (the dashed red line in Figure 6a):

$$G_0 = 76.7 + 3.6 \times X_F - 0.8 \times X_{Fe} \quad (15)$$

where X_{Fe} = Fe/(Ti+Fe+Mg). We further explore the influence of H_2O content on the elasticity of clinohumite at ambient conditions. Both K_{S0} and G_0 of clinohumite follow a linear decrease with increasing H_2O content when the Fe content is less than 1.1 mol.% (the solid red lines in Figure 6b):

$$K_{S0} = 131.2(46) - 4.1(21) \times C_{H_2O} \quad (16)$$

$$G_0 = 80.0(32) - 1.1(14) \times C_{H_2O} \quad (17)$$

where C_{H_2O} is the weight percentage of H_2O in clinohumite. Increasing the Fe content causes a reduction in the G_0 but has a minor effect on the K_{S0}. The net effect of Fe and H_2O content on the G_0 of clinohumite can be expressed as (the dash red line in Figure 6b):

$$G_0 = 80.0 - 1.1 \times C_{H_2O} - 0.8 \times X_{Fe} \quad (18)$$

Humite

Our study reports experimental constraints on the elastic properties of orthorhombic humite (Table 3). The elastic constants of our humite sample (F_{37}-Hu) show $C_{22}>C_{11}>C_{33}$ and $C_{66}\approx C_{44}>C_{55}$, which are similar to clinohumite. This indicates that humite shares the same axial compressional ($\beta_c>\beta_a>\beta_b$) and shear elastic properties as clinohumite. In humite, as in clinohumite, the key structural units contain jagged chains of edge-sharing MO_6-octahedra and two distinct SiO_4-tetrahedra (Figure 2b) (Ribbe and Gibbs, 1971). And likewise, since the SiO_4-tetrahedra are arranged in the *b*-direction, the *b*-direction is the stiffest. Moreover, the anisotropy of humite also exhibits a similar pattern to clinohumite, with the fastest P-wave propagating

along the *b*-axis direction (polarization [010]) and the highest S-wave splitting at ~45° between the *a*- and *b*-axes. Furthermore, it is interesting to note that both K_{S0} and G_0 of humite follow the same trends with increasing H_2O content as clinohumite (the solid red lines in Figures 6a and 6b).

Chondrodite

In Table 3, we summarized the elasticity of chondrodite with varying compositions (Sinogeikin and Bass, 1999; Ye et al., 2015). Our Fe-free F_{61}-chondrodite exhibits $\beta_a>\beta_c>\beta_b$ ($C_{22}>C_{33}>C_{11}$). This is consistent with previous experimental results for OH-chondrodite with or without Fe (Kuribayashi et al., 2004; Ross and Crichton, 2001; Ye et al., 2015). In contrast, the net effect of F and Fe tends to enhance the incompressibility of chondrodite along the *a*-axis (C_{11}), leading to $\beta_c>\beta_a>\beta_b$ ($C_{22}>C_{11}>C_{33}$) (Friedrich et al., 2002; Kuribayashi et al., 2004; Sinogeikin and Bass, 1999). For the shear moduli, our Fe-free chondrodite (F_{61}-Chn) has $C_{66}\approx C_{44}>C_{55}$, while Fe-bearing chondrodite samples exhibit $C_{66}>C_{55}>C_{44}$ (Sinogeikin and Bass, 1999; Ye et al., 2015). By combining the elasticity and density, we calculated the velocity anisotropy of the chondrodite (Table 3). The P-wave velocity anisotropy of chondrodite is similar to clinohumite, with the fastest P-wave propagating along the *b*-axis direction (polarization [010]), whereas it has the highest AV_S along the [111] direction. And compared to clinohumite, chondrodite has a slightly lower AV_P but similar AV_S (Fritzel and Bass, 1997; Sinogeikin and Bass, 1999; Ye et al., 2015).

We compared the elastic moduli of chondrodite with varying compositions determined by Brillouin scattering (Table 3) (Sinogeikin and Bass, 1999; Ye et al., 2015). The limited sensitivity of K_{S0} to Fe content may be attributed to the weak impact of Fe substitution on the M-O bond length (unit cell volume) (Ye et al., 2015; Ye et al., 2013). Moreover, in some minerals

311 within the MSH system, the presence of a small amount of Fe (less than 10 mol%) has a minimal
312 effect on the bulk modulus, such as olivine and orthopyroxene (Jackson et al., 1999; Nestola et
313 al., 2011). Therefore, the K_{S0} is nearly independent of the Fe content and exhibits a linear
314 increase (decrease) with the F (H_2O) content (the solid blue lines in Figure 6a):

315 $$K_{S0} = 117.6(10) + 3.9(24) \times X_F \quad (19)$$

316 $$K_{S0} = 121.3(18) - 0.7(5) \times C_{H2O} \quad (20)$$

317 These trends suggest that Fe content has a negligible effect on the K_{S0} of chondrodite. However,
318 G_0 of chondrodite with 5.4 mol% Fe is unusually greater than the corresponding Fe-free phase
319 with the same H_2O content estimated from the linear trend in Figure 6 (Sinogeikin and Bass,
320 1999). Due to limited experimental data and great anomalous G_0 of chondrodite with 5.4 mol%
321 Fe, future studies are expected to provide more reliable constraints on the influence of the net
322 effect of Fe and H_2O on the elasticity of chondrodite.

323

324 **Humite-group minerals**

325 We further investigated the relationship between sound velocity and H_2O content for humite-
326 group minerals (Figure 6c). Regardless of the specific structure, compressional (V_P) and shear-
327 wave (V_S) velocities of all the humite-group minerals follow the same linear decrease with
328 increasing H_2O content when the Fe content is less than 1.1 mol% (Fritzel and Bass, 1997;
329 Sinogeikin and Bass, 1999; Ye et al., 2015) (the solid grey lines in Figure 6c):

330 $$V_P = 8.51(5) - 0.05(2) \times C_{H2O} \quad (21)$$

331 $$V_S = 5.02(5) - 0.05(2) \times C_{H2O} \quad (22)$$

332 These linear relationships between H_2O content and sound velocities indicate that composition
333 instead of structure plays the dominant role in the sound velocity of humite-group minerals.

This is the peer-reviewed, final accepted version for American Mineralogist, published by the Mineralogical Society of America.
The published version is subject to change. Cite as Authors (Year) Title. American Mineralogist, in press.
DOI: https://doi.org/10.2138/am-2023-9067. http://www.minsocam.org/

Besides H_2O content, Fe is the other factor causing a further reduction in sound velocity. Since the experimental data are limited, here we provide preliminary estimations on the combined effect of H_2O and Fe content on the V_P and V_S of humite-group minerals (the dash lines in Figure 6c):

$$V_P = 8.51 - 0.05 \times C_{H_2O} - 0.02(1) \times X_{Fe} \quad (23)$$

$$V_S = 5.02 - 0.05 \times C_{H_2O} - 0.04(1) \times X_{Fe} \quad (24)$$

IMPLICATIONS

A previous study has shown that the substitution of fluorine for hydroxyl can significantly expand the temperature stability of clinohumite above the normal mantle geotherm at high pressures (Grützner et al., 2017). Clinohumite, as well as other humite-group minerals, could be important water and fluorine carriers to the Earth's deep mantle, and if found within the Earth's interior, they are likely to be present in lithospheric material that gets subducted down to (potentially) transition zone depths (Akimoto et al., 1977; Engi and Lindsley, 1980; Grützner et al., 2017; Rice, 1980). Here, we compared the sound velocity of measured humite-group minerals to that of major mantle minerals. Although our obtained results are at ambient conditions, such comparison provides important insights into the influence of humite-minerals on the mantle velocity structure.

At ambient conditions, all of our measured humite-group minerals have a similar V_P to that of olivine (Figure 7). The difference in V_P between our measured humite-group minerals and olivine is within 1.8% (Mao et al., 2015). Our measured humite-group minerals have V_P 4.5-6.9%

and 3-5.3% greater than orthopyroxene and clinopyroxene, respectively, but their V_P is 5.5-7.7% lower than garnet (Li and Neuville, 2010; Li et al., 2022; Wei et al., 2021). The difference in V_S among our measured humite-group minerals and upper mantle minerals is within 5.7%. Considering a maximum volume percentage of 8 vol.%, the presence of humite-group minerals in the upper mantle might have a weak effect on the upper mantle velocity structure. As noted above, the addition of F can greatly expand the stability pressure and temperature range of clinohumite in the Earth's mantle. Clinohumite can remain stable in the mantle transition zone when F concentration exceeds ~0.45. Here, we have shown that under ambient conditions, although the V_S of F_{45}-clinohumite is only 1.2% lower than majoritic garnet, its V_P is 4.6-9.3% lower than wadsleyite and majoritic garnet (Mao et al., 2015; Wei et al., 2021). The difference in V_S between F_{45}-clinohumite and wadsleyite is as large as 9.5%. In this case, the presence of clinohumite could lead to a substantial decrease in the mantle transition zone velocity.

In addition, compared to other hydrous phases in the upper mantle, such as phases A and E, humite-group minerals exhibit higher V_P and V_S (Figure 7). In the Fe-free system, OH-chondrodite displays the lowest sound velocities (V_P=8.25(12) km/s and V_S=4.76(12) km/s) within the humite-group minerals at ambient conditions. Despite these relatively low values within the humite-group minerals, the V_P of chondrodite still exceeds that of Fe-free phase A by 2.9%, and its V_P and V_S are 5.8% and 4.6% higher than those of Fe-free phase E, respectively (Cai et al., 2021; Wang et al., 2022). Incorporation of Fe will lead to a reduction in both V_P and V_S of chondrodite, phase A, and phase E (Sanchez-Valle et al., 2006; Satta et al., 2019). Addition of 1 mol.% Fe lowers the V_P and V_S of chondrodite by 0.2% and 0.8%. In comparison, the same amount of Fe can produce a 0.6% and 2.3% reduction in the V_P and V_S for phase A and a 0.3%

This is the peer-reviewed, final accepted version for American Mineralogist, published by the Mineralogical Society of America.
The published version is subject to change. Cite as Authors (Year) Title. American Mineralogist, in press.
DOI: https://doi.org/10.2138/am-2023-9067. http://www.minsocam.org/

reduction in both V_P and V_S for phase E. In this case, the presence of Fe has a greater effect on the sound velocity of phase A than chondrodite and phase E.

The humite-group minerals [$nMg_2SiO_4 \cdot Mg(OH)_2$] consist of a series of phases along the forsterite-brucite join in the MgO-SiO_2-H_2O system. Along this join, the composition has been shown to play a more relevant role in determining the elasticity and sound velocities than structure (Jacobsen et al., 2008; Kuribayashi et al., 2008; Ross and Crichton, 2001; Sanchez-Valle et al., 2006; Ye et al., 2015). The relationships between H_2O content and density (elastic moduli and velocity) of various phases along the forsterite-brucite join have been reported in previous studies (Sanchez-Valle et al., 2006; Ye et al., 2015). Here, we combined the data of humite-group minerals determined in this study together with those of phase A, forsterite, and brucite along the forsterite-brucite join to plot a more explicit trend (Figure 8). Increasing H_2O content from anhydrous forsterite to brucite leads to a substantial decrease in density, elasticity, and sound velocities. The relationship between H_2O content and density (elastic moduli and sound velocities) derived here is consistent with previous studies (Sanchez-Valle et al., 2006; Ye et al., 2015):

$$\rho = 3.23(1) - 0.027(1) \times C_{H_2O} \quad (25)$$

$$K_{S0} = 128.5(8) - 2.66(5) \times C_{H_2O} \quad (26)$$

$$G_0 = 81.1(6) - 1.49(4) \times C_{H_2O} \quad (27)$$

$$V_P = 8.61(3) - 0.075(3) \times C_{H_2O} \quad (28)$$

$$V_S = 5.03(1) - 0.038(1) \times C_{H_2O} \quad (29)$$

On the opposite, elasticity and sound velocities of phases along the forsterite-brucite join exhibit a linear increase with increasing density, which can be expressed as (Figure 9):

This is the peer-reviewed, final accepted version for American Mineralogist, published by the Mineralogical Society of America.
The published version is subject to change. Cite as Authors (Year) Title. American Mineralogist, in press.
DOI: https://doi.org/10.2138/am-2023-9067. http://www.minsocam.org/

403 $$K_{S0} = 98.0(17) \times \rho - 188.1(53) \quad (30)$$

404 $$G_0 = 54.9(13) \times \rho - 96.1(40) \quad (31)$$

405 $$V_P = 2.79(7) \times \rho - 0.40(22) \quad (32)$$

406 $$V_S = 1.40(4) \times \rho - 0.51(12) \quad (33)$$

407

408 Along the forsterite-brucite join when the Fe content is less than 5 mol.%, the addition of Fe was
409 noted to have a weak effect on the density, elasticity, and sound velocities at a given H_2O content
410 (Figure 8). But when we plot the elastic moduli (sound velocities) of phases along the forsterite-
411 brucite join as a function of density, the presence of Fe causes an obvious offset of the elasticity
412 (sound velocity) to lower values. Regardless the specific Fe content, the relationship between
413 density and elastic moduli (sound velocities) for these Fe-bearing phases can be expressed as:

414 $$K_{S0} = 60.3(44) \times \rho - 72(15) \quad (34)$$

415 $$G_0 = 42.5(45) \times \rho - 63(15) \quad (35)$$

416 $$V_P = 0.95(17) \times \rho + 5.2(6) \quad (36)$$

417 $$V_S = 0.64(17) \times \rho + 2.7(5) \quad (37)$$

418 The experimental results obtained in this study are valuable to provide better constraints on the
419 elasticity of humite-group minerals and confirm the previous observations along the brucite-
420 forsterite join (Sanchez-Valle et al., 2006; Ye et al., 2015). Additionally, to determine the
421 specific impact of Fe content on the elastic properties of phases along the forsterite-brucite join,
422 it is necessary to have more elasticity data for Fe-bearing samples in future studies.

423

424

425

426

427 ## ACKNOWLEDGEMENTS

428 We thank the support of Wancai Li in conducting the EMPA measurements. We also appreciate
429 the assistance of Haipeng Song in the XRD measurements under ambient conditions. The XRD
430 data were collected using a Bruker D8 QUEST X-ray single crystal diffraction instrument at the
431 State Key Laboratory of Geological Processes and Mineral Resources, China University of
432 Geosciences, Wuhan.

433

434 ## FUNDING

435 This work is supported by the China National Science Foundation (42241117 and 42272036) and
436 the Fundamental Research Funds for the Central Universities (WK2080000144).

437

REFERENCES CITED

Abramson, E.H., Brown, J.M., Slutsky, L.J., and Zaug, J. (1997) The elastic constants of San Carlos olivine to 17 GPa. Journal of Geophysical Research: Solid Earth, 102(B6), 12253-12263.

Akimoto, S., Yamamoto, K., and Aoki, K. (1977) Hydroxyl-clinohumite and hydroxyl-chondrodite: Possible H_2O-bearing minerals in the upper mantle. In M.H. Manghnani, and S.-I. Akimoto, Eds. High-Pressure Research, p. 163-172.

Bass, J.D., Weidner, D.J., Hamaya, N., Ozima, M., and Akimoto, S. (1984) Elasticity of the olivine and spinel polymorphs of Ni_2SiO_4. Physics and Chemistry of Minerals, 10(6), 261-272.

Berry, A.J., and James, M. (2001) Refinement of hydrogen positions in synthetic hydroxyl-clinohumite by powder neutron diffraction. American Mineralogist, 86(1-2), 181-184.

Brown, J.M. (2018) Determination of elastic moduli from measured acoustic velocities. Ultrasonics, 90, 23-31.

Brown, J.M., Slutsky, L.J., Nelson, K.A., and Cheng, L.-T. (1989) Single-crystal elastic constants for San Carlos peridot: An application of impulsive stimulated scattering. Journal of Geophysical Research, 94(B7), 9485-9492.

Burnley, P.C., and Navrotsky, A. (1996) Synthesis of high-pressure hydrous magnesium silicates; observations and analysis. American Mineralogist, 81(3-4), 317-326.

Cai, N., Qi, X., Chen, T., Wang, S., Yu, T., Wang, Y., Inoue, T., Wang, D., and Li, B. (2021) Enhanced Visibility of Subduction Slabs by the Formation of Dense Hydrous Phase A. Geophysical Research Letters, 48(19), e2021GL095487.

Camara, F. (1997) New data on the structure of norbergite; location of hydrogen by X-ray diffraction. The Canadian Mineralogist, 35(6), 1523-1530.

Darling, K.L., Gwanmesia, G.D., Kung, J., Li, B., and Liebermann, R.C. (2004) Ultrasonic measurements of the sound velocities in polycrystalline San Carlos olivine in multi-anvil, high-pressure apparatus. Physics of the Earth and Planetary Interiors, 143-144, 19-31.

Dasgupta, R., and Hirschmann, M.M. (2010) The deep carbon cycle and melting in Earth's interior. Earth and Planetary Science Letters, 298(1-2), 1-13.

Dixon, J.E., Leist, L., Langmuir, C., and Schilling, J.-G. (2002) Recycled dehydrated lithosphere observed in plume-influenced mid-ocean-ridge basalt. Nature, 420(6914), 385-389.

Ehlers, K., and Hoinkes, G. (1987) Titanian chondrodite and clinohumite in marbles from the tztal crystalline basement. Mineralogy Petrology, 36(1), 13-25.

Engi, M., and Lindsley, D.H. (1980) Stability of titanian clinohumite: Experiments and thermodynamic analysis. Contributions to Mineralogy and Petrology, 72(4), 415-424.

Evans, B.W., and Trommsdorff, V. (1983) Fluorine hydroxyl titanian clinohumite in Alpine recrystallized garnet peridotite: compositional controls and petrologic significance. American Journal of Science, 283, 355-369.

Every, A. (1980) General closed-form expressions for acoustic waves in elastically anisotropic solids. Physical Review B, 22(4), 1746-1760.

Faccincani, L., Criniti, G., Kurnosov, A., Ballaran, T.B., Withers, A.C., Mazzucchelli, M., Nestola, F., and Coltorti, M. (2023) Sound velocities and single-crystal elasticity of hydrous Fo90 olivine to 12 GPa. Physics of the Earth and Planetary Interiors, 337, https://doi.org/10.1016/j.pepi.2023.107011.

Ferraris, G., Prencipe, M., Sokolova, E., Gekimyants, V.M., and Spiridonov, E.M. (2000) Hydroxylclinohumite, a new member of the humite group: Twinning, crystal structure and crystal chemistry of the clinohumite subgroup. 215(3), 169-173.

Finger, L.W., Hazen, R.M., and Prewitt, C.T. (1991) Crystal structures of $Mg_{12}Si_4O_{19}(OH)_2$ (phase B) and $Mg_{14}Si_5O_{24}$ (phase AnhB). American Mineralogist, 76(1-2), 1-7.

Flemetakis, S., Tiraboschi, C., Rohrbach, A., Berndt, J., and Klemme, S. (2022) The stability of antigorite in subduction zones revisited: the effect of F on antigorite stability and its breakdown reactions at high pressures and high temperatures, with implications for the geochemical cycles of halogens. Contributions to Mineralogy and Petrology, 177(7), https://doi.org/10.1007/s00410-022-01934-5.

Friedrich, A., Lager, G.A., Ulmer, P., Kunz, M., and Marshall, W.G. (2002) High-pressure single-crystal X-ray and powder neutron study of F,OH/OD-chondrodite: Compressibility, structure, and hydrogen bonding. American Mineralogist, 87(7), 931-939.

Fritzel, T.L.B., and Bass, J.D. (1997) Sound velocities of clinohumite, and implications for water in Earth's upper mantle. Geophysical Research Letters, 24(9), 1023-1026.

Grützner, T., Klemme, S., Rohrbach, A., Gervasoni, F., and Berndt, J. (2017) The role of F-clinohumite in volatile recycling processes in subduction zones. Geology, 45(5), 443-446.

Hermann, J., Fitz Gerald, J.D., Malaspina, N., Berry, A.J., and Scambelluri, M. (2007) OH-bearing planar defects in olivine produced by the breakdown of Ti-rich humite minerals from Dabie Shan (China). Contributions to Mineralogy and Petrology, 153(4), 417-428.

Hill, R. (1963) Elastic properties of reinforced solids: Some theoretical principles. Journal of the Mechanics and Physics of Solids, 11(5), 357-372.

Holl, C.M., Smyth, J.R., Manghnani, M.H., Amulele, G.M., Sekar, M., Frost, D.J., Prakapenka, V.B., and Shen, G. (2006) Crystal structure and compression of an iron-bearing Phase A to 33 GPa. Physics and Chemistry of Minerals, 33(3), 192-199.

Hou, M., Zhou, W.-Y., Hao, M., Hua, F.T.-S., Kung, J., Zhang, D., Dera, P.K., and Zhang, J.S. (2022) Effect of structural water on the elasticity of orthopyroxene. American Mineralogist, 107(4), 703-708.

Hughes, L., and Pawley, A. (2019) Fluorine partitioning between humite-group minerals and aqueous fluids: implications for volatile storage in the upper mantle. Contributions to Mineralogy Petrology, 174(9), https://doi.org/10.1007/s00410-019-1614-2.

Hushur, A., Manghnani, M.H., Smyth, J.R., Nestola, F., and Frost, D.J. (2009) Crystal chemistry of hydrous forsterite and its vibrational properties up to 41 GPa. American Mineralogist, 94(5-6), 751-760.

Isaak, D.G., Anderson, O.L., Goto, T., and Suzuki, I. (1989) Elasticity of single-crystal forsterite measured to 1700 K. 94(B5), 5895-5906.

Isaak, D.G., Graham, E.K., Bass, J.D., and Wang, H. (1993) The elastic properties of single-crystal fayalite as determined by dynamical measurement techniques. pure and applied geophysics, 141(2), 393-414.

Iwamori, H. (2004) Phase relations of peridotites under H_2O-saturated conditions and ability of subducting plates for transportation of H_2O. Earth and Planetary Science Letters, 227(1-2), 57-71.

Jackson, J.M., Sinogeikin, S.V., and Bass, J.D. (1999) Elasticity of $MgSiO_3$ orthoenstatite. American Mineralogist, 84(4), 677-680.

Jacobsen, S.D., Jiang, F., Mao, Z., Duffy, T.S., Smyth, J.R., Holl, C.M., and Frost, D.J. (2008) Effects of hydration on the elastic properties of olivine. Geophysical Research Letters, 35(14), 559-568.

Jiang, F., Speziale, S., and Duffy, T.S. (2006) Single-crystal elasticity of brucite, $Mg(OH)_2$, to 15 GPa by Brillouin scattering. American Mineralogist, 91(11-12), 1893-1900.

Kaminsky, F. (2012) Mineralogy of the lower mantle: A review of 'super-deep' mineral inclusions in diamond. Earth-Science Reviews, 110(1-4), 127-147.

Karki, B.B., Stixrude, L., and Wentzcovitch, R.M. (2001) High-pressure elastic properties of major materials of Earth's mantle from first principles. Reviews of Geophysics, 39(4), 507-534.

Kobayashi, M., Sumino, H., Nagao, K., Ishimaru, S., Arai, S., Yoshikawa, M., Kawamoto, T., Kumagai, Y., Kobayashi, T., Burgess, R., and Ballentine, C.J. (2017) Slab-derived halogens and noble gases illuminate closed system processes controlling volatile element transport into the mantle wedge. Earth and Planetary Science Letters, 457, 106-116.

Komabayashi, T., Omori, S., and Maruyama, S. (2005) Experimental and theoretical study of stability of dense hydrous magnesium silicates in the deep upper mantle. Physics of the Earth Planetary Interiors, 153(4), 191-209.

Kudoh, Y., Inoue, T., and Arashi, H. (1996) Structure and crystal chemistry of hydrous wadsleyite, Mg1.75SiH0.5O4: possible hydrous magnesium silicate in the mantle transition zone. Physics and Chemistry of Minerals, 23(7), 461-469.

Kuribayashi, T., Kagi, H., Tanaka, M., Akizuki, M., and Kudoh, Y. (2004) High-pressure single crystal X-ray diffraction and FT-IR observation of natural chondrodite and synthetic OH-chondrodite. Journal of Mineralogical & Petrological Sciences, 99(3), 118-129.

Kuribayashi, T., Tanaka, M., and Kudoh, Y. (2008) Synchrotron X-ray analysis of norbergite, $Mg_{2.98}Fe_{0.01}Ti_{0.02}Si_{0.99}O_4(OH_{0.31}F_{1.69})$ structure at high pressure up to 8.2 GPa. Physics and Chemistry of Minerals, 35(10), 559-568.

Lager, G.A., Ulmer, P., Miletich, R., and Marshall, W.G. (2001) O-D···O bond geometry in OD-chondrodite. American Mineralogist, 86(1-2), 176-180.

Li, B., Kung, J., and Liebermann, R.C. (2004) Modern techniques in measuring elasticity of Earth materials at high pressure and high temperature using ultrasonic interferometry in conjunction with synchrotron X-radiation in multi-anvil apparatus. Physics of the Earth and Planetary Interiors, 143-144, 559-574.

Li, B., and Neuville, D.R. (2010) Elasticity of diopside to 8GPa and 1073K and implications for the upper mantle. Physics of the Earth and Planetary Interiors, 183(3-4), 398-403.

Li, L., Sun, N., Shi, W., Mao, Z., Yu, Y., Zhang, Y., and Lin, J.F. (2022) Elastic Anomalies Across the α-β Phase Transition in Orthopyroxene: Implication for the Metastable Wedge in the Cold Subduction Slab. Geophysical Research Letters, 49(16).

Lindsay, S.M., Anderson, M.W., and Sandercock, J.R. (1981) Construction and alignment of a high performance multipass vernier tandem Fabry–Perot interferometer. Review of Scientific Instruments, 52(10), 1478-1486.

Liu, D., Hirner, S.M., Smyth, J.R., Zhang, J., Shi, X., Wang, X., Zhu, X., and Ye, Y. (2021) Crystal chemistry and high-temperature vibrational spectra of humite and norbergite: Fluorine and titanium in humite-group minerals. American Mineralogist, 106(7), 1153-1162.

Liu, W., Kung, J., and Li, B. (2005) Elasticity of San Carlos olivine to 8 GPa and 1073 K. Geophysical Research Letters, 32(16), https://doi.org/10.1029/2005GL023453.

Mao, Z., Fan, D., Lin, J.-F., Yang, J., Tkachev, S.N., Zhuravlev, K., and Prakapenka, V.B. (2015) Elasticity of single-crystal olivine at high pressures and temperatures. Earth and Planetary Science Letters, 426, 204-215.

Momma, K., and Izumi, F. (2011) VESTA 3 for three-dimensional visualization of crystal, volumetric and morphology data. Journal of applied crystallography, 44(6), 1272-1276.

Mookherjee, M., and Stixrude, L. (2009) Structure and elasticity of serpentine at high-pressure. Earth and Planetary Science Letters, 279(1), 11-19.

Nagai, T., Hattori, T., and Yamanaka, T. (2000) Compression mechanism of brucite: An investigation by structural refinement under pressure. American Mineralogist, 85(5-6), 760-764.

Nestola, F., Pasqual, D., Smyth, J.R., Novella, D., Secco, L., Manghnani, M.H., and Dal Negro, A. (2011) New accurate elastic parameters for the forsterite-fayalite solid solution. American Mineralogist, 96(11-12), 1742-1747.

Nishi, M., Irifune, T., Tsuchiya, J., Tange, Y., Nishihara, Y., Fujino, K., and Higo, Y. (2014) Stability of hydrous silicate at high pressures and water transport to the deep lower mantle. Nature Geoscience, 7(3), 224-227.

Nye, J.F. (1957) Physical properties of crystals : their representation by tensors and matrices. Clarendon Press.

Ohtani, E., Amaike, Y., Kamada, S., Sakamaki, T., and Hirao, N. (2014) Stability of hydrous phase H MgSiO4H2 under lower mantle conditions. 41(23), 8283-8287.

Ohtani, E., Shibata, T., Kubo, T., and Kato, T. (1995) Stability of hydrous phases in the transition zone and the upper most part of the lower mantle. 22(19), 2553-2556.

Ohtani, E., Yuan, L., Ohira, I., Shatskiy, A., and Litasov, K. (2018) Fate of water transported into the deep mantle by slab subduction. Journal of Asian Earth Sciences, 167, 2-10.

Phan, H.T. (2008) Elastic properties of hydrous phases in the deep mantle: high-pressure ultrasonic wave velocity measurements on clinohumite and phase A, Doctor of Natural Science ETH Zurich.

Qin, F., Wu, X., Zhang, D., Qin, S., and Jacobsen, S.D. (2017) Thermal Equation of State of Natural Ti-Bearing Clinohumite. Journal of Geophysical Research Solid Earth, 122(11), 8943-8951.

Rashchenko, S.V., Kamada, S., Hirao, N., Litasov, K.D., and Ohtani, E. (2016) In situ X-ray observation of 10 Å phase stability at high pressure. 101(11), 2564-2569.

Ribbe, P.H., and Gibbs, G.V. (1971) Crystal Structures of the Humite Minerals: III. Mg/Fe Ordering in Humite and its Relation to Other Ferromagnesian Silicates. American Mineralogist, 56(7-8), 1155-1173.

Rice, J.M. (1980) Phase equilibria involving humite minerals in impure dolomitic limestones. Contributions to Mineralogy Petrology, 71(3), 219-235.

Robinson, K., Gibbs, G.V., and Ribbe, P.H. (1973) The crystal structures of the humite minerals. IV. Clinohumite and titanoclinohumite. American Mineralogist, 58(1-2), 43-49.

Ross, N.L., and Crichton, W.A. (2001) Compression of synthetic hydroxylclinohumite [$Mg_9Si_4O_{16}(OH)_2$] and hydroxylchondrodite [$Mg_5Si_2O_8(OH)_2$]. American Mineralogist, 86(9), 990-996.

Sanchez-Valle, C., and Bass, J.D. (2010) Elasticity and pressure-induced structural changes in vitreous MgSiO3-enstatite to lower mantle pressures. Earth and Planetary Science Letters, 295(3), 523-530.

Sanchez-Valle, C., Sinogeikin, S.V., Smyth, J.R., and Bass, J.D. (2006) Single-crystal elastic properties of dense hydrous magnesium silicate phase A. American Mineralogist, 91(5-6), 961-964.

Sandercock, J.R. (1982) Trends in brillouin scattering: Studies of opaque materials, supported films, and central modes. Topics in Applied Physics, 173-206.

Satta, N., Marquardt, H., Kurnosov, A., Buchen, J., Kawazoe, T., McCammon, C., and Ballaran, T.B. (2019) Single-crystal elasticity of iron-bearing phase E and seismic detection of water in Earth's upper mantle. American Mineralogist, 104(10), 1526-1529.

Scarponi, F., Mattana, S., Corezzi, S., Caponi, S., Comez, L., Sassi, P., Morresi, A., Paolantoni, M., Urbanelli, L., Emiliani, C., Roscini, L., Corte, L., Cardinali, G., Palombo, F., Sandercock, J.R., and Fioretto, D. (2017) High-Performance Versatile Setup for Simultaneous Brillouin-Raman Microspectroscopy. Physical Review X, 7(3), 031015.

Selyatitskii, A.Y., and Reverdatto, V.V. (2022) Thermobaric Conditions for Exhumation of Ti-clinohumite Garnetites of the Kokchetav Subduction-Collision Zone (Northern Kazakhstan). Russian Geology and Geophysics, 63(8), 869-889.

Shen, T., Hermann, J., Zhang, L., Lü, Z., Padrón-Navarta, J.A., Xia, B., and Bader, T. (2015) UHP Metamorphism Documented in Ti-chondrodite- and Ti-clinohumite-bearing Serpentinized Ultramafic Rocks from Chinese Southwestern Tianshan. Journal of Petrology, 56(7), 1425-1458.

Shimizu, H., and Sasaki, S. (1992) High-Pressure Brillouin Studies and Elastic Properties of Single-Crystal H_2S Grown in a Diamond Cell. Science, 257(5069), 514-516.

Sinogeikin, S., Bass, J., Prakapenka, V., Lakshtanov, D., Shen, G., Sanchez-Valle, C., and Rivers, M. (2006) Brillouin spectrometer interfaced with synchrotron radiation for simultaneous x-ray density and acoustic velocity measurements. Review of Scientific Instruments, 77(10).

Sinogeikin, S., and Bass, J.D. (1999) Single-crystal elastic properties of chondrodite: implications for water in the upper mantle. Physics Chemistry of Minerals, 26(4), 297-303.

Sinogeikin, S.V., and Bass, J.D. (2000) Single-crystal elasticity of pyrope and MgO to 20 GPa by Brillouin scattering in the diamond cell. Physics of the Earth Planetary Interiors, 120(1-2), 43-62.

Sinogeikin, S.V., Katsura, T., and Bass, J.D. (1998) Sound velocities and elastic properties of Fe-bearing wadsleyite and ringwoodite. Journal of Geophysical Research: Solid Earth, 103(B9), 20819-20825.

Smyth, J.R., Frost, D.J., Nestola, F., Holl, C.M., and Bromiley, G. (2006) Olivine hydration in the deep upper mantle: Effects of temperature and silica activity. Geophysical Research Letters, 33(15), 311-324.

Speziale, S., Duffy, T.S., and Angel, R.J. (2004) Single-crystal elasticity of fayalite to 12 GPa. Journal of Geophysical Research, 109(B12), https://doi.org/10.1029/2004JB003162.

Speziale, S., Marquardt, H., Duffy, T.S.J.R.i.M., and Geochemistry. (2014) Brillouin scattering and its application in geosciences. 78(1), 543-603.

Stalder, R., and Ulmer, P. (2001) Phase relations of a serpentine composition between 5 and 14 GPa: significance of clinohumite and phase E as water carriers into the transition zone. Contributions to Mineralogy Petrology, 140(6), 670-679.

Stixrude, L. (2002) Talc under tension and compression: Spinodal instability, elasticity, and structure. 107(B12), ECV 2-1-ECV 2-10.

Sumino, Y. (1979) The elastic constants of Mn_2SiO_4, Fe_2SiO_4 and Co_2SiO_4, and the elastic properties of olivine group minerals at high temperature. Journal of Physics of the Earth, 27(3), 209-238.

Suzuki, I., Anderson, O.L., and Sumino, Y. (1983) Elastic properties of a single-crystal forsterite Mg_2SiO_4, up to 1,200 K. Physics Chemistry of Minerals, 10(1), 38-46.

Thompson, A.B. (1992) Water in the Earth's upper mantle. Nature, 358(6384), 295-302.

Wang, B., Zhang, Y., Fu, S., Ding, X., Liang, W., Takahashi, E., Li, L., Tkachev, S.N., Prakapenka, V.B., and Lin, J.F. (2022) Single-crystal elasticity of phase E at high pressure and temperature: Implications for the low-velocity layer atop the 410-km depth. Journal of Geophysical Research: Solid Earth, 107(1), 147-152.

Wang, J. (2008) The effect of hydration state, Fe, and spin state of Fe on the elasticity of mantle minerals at high pressure. Geology, Ph.D. University of Illinois at Urbana-Champaign.

Waters, L.E., Cottrell, E., Coombs, M.L., and Kelley, K.A. (2021) Generation of Calc-Alkaline Magmas during Crystallization at High Oxygen Fugacity: An Experimental and Petrologic Study of Tephras from Buldir Volcano, Western Aleutian Arc, Alaska, USA. Journal of Petrology, 62(3).

Webb, S.L. (1989) The elasticity of the upper mantle orthosilicates olivine and garnet to 3 GPa. Physics and Chemistry of Minerals, 16(7), 684-692.

Webb, S.L., and Jackson, I. (1990) Polyhedral rationalization of variation among the single-crystal elastic moduli for the upper-mantle silicates garnet, olivine, and orthopyroxene. American Mineralogist, 75(7-8), 731-738.

Wei, W., Mao, Z., Sun, N., Sun, D., and Tkachev, S.N. (2021) High Pressure-Temperature Single-Crystal Elasticity of Grossular: Implications for the Low-Velocity Layer in the Bottom Transition Zone. Geophysical Research Letters, 48(9).

Whitfield, C.H., Brody, E.M., and Bassett, W.A. (1976) Elastic moduli of NaCl by Brillouin scattering at high pressure in a diamond anvil cell. Review of Scientific Instruments, 47(8), 942-947.

Wirth, R., Kaminsky, F., Matsyuk, S., and Schreiber, A. (2009) Unusual micro- and nano-inclusions in diamonds from the Juina Area, Brazil. Earth and Planetary Science Letters, 286(1-2), 292-303.

Wunder, B. (1998) Equilibrium experiments in the system MgO-SiO_2-H_2O (MSH): stability fields of clinohumite-OH [$Mg_9Si_4O_{16}(OH)_2$], chondrodite-OH [$Mg_5Si_2O_8(OH)_2$] and phase A ($Mg_7Si_2O_8OH)_6$). Contributions to Mineralogy and Petrology, 132(2), 111-120.

Xia, X., Weidner, D.J., and Zhao, H. (1998) Equation of state of brucite: Single-crystal Brillouin spectroscopy study and polycrystalline pressure-volume-temperature measurement. American Mineralogist, 83(1), 68-74.

Yamamoto, K., and Akimoto, S. (1977) The system MgO-SiO_2-H_2O at high pressures and temperatures; stability field for hydroxyl-chondrodite, hydroxyl-clinohumite and 10 Å-phase. American Journal of Science, 277(3), 288-312.

Ye, Y., Jacobsen, S.D., Mao, Z., Duffy, T.S., Hirner, S.M., and Smyth, J.R. (2015) Crystal structure, thermal expansivity, and elasticity of OH-chondrodite: trends among dense hydrous magnesium silicates. Contributions to Mineralogy & Petrology, 169(4), https://doi.org/10.1007/s00410-015-1138-3.

Ye, Y., R.Smyth, J., D.Jacobsen, S., and Goujon, C. (2013) Crystal chemistry, thermal expansion, and Raman spectra of hydroxyl-clinohumite: implications for water in Earth's interior. Contributions to Mineralogy Petrology, 165(3), 563-574.

Zaug, J.M., Abramson, E.H., Brown, J.M., and Slutsky, L.J. (1993) Sound Velocities in Olivine at Earth Mantle Pressures. 260(5113), 1487-1489.

Zha, C.-S., Duffy, T.S., Downs, R.T., Mao, H.-K., and Hemley, R.J. (1996) Sound velocity and elasticity of single-crystal forsterite to 16 GPa. Journal of Geophysical Research: Solid Earth, 101(B8), 17535-17545.

Zha, C.-s., Duffy, T.S., Downs, R.T., Mao, H.-k., and Hemley, R.J. (1998) Brillouin scattering and X-ray diffraction of San Carlos olivine: direct pressure determination to 32 GPa. Earth Planetary Science Letters, 159(1-2), 25-33.

Zhang, J., Wang, S., Chen, S., Li, B., and Liu, Q. (2023) Sound velocities of natural clinohumite at high pressures and implications for seismic velocities of subducted slabs in the upper mantle. Physics of the Earth and Planetary Interiors, 341.

Zouboulis, I.S., Jiang, F., Wang, J., and Duffy, T.S. (2014) Single-crystal elastic constants of magnesium difluoride (MgF2) to 7.4GPa. Journal of Physics and Chemistry of Solids, 75(1), 136-141.

FIGURE 1. Composition of minerals in the MgO-SiO_2-H_2O system. A: phase A (Holl et al., 2006); Ahy B: anhydrous phase B (Finger et al., 1991); B: phase B (Finger et al., 1991); Br: brucite (Nagai et al., 2000); Chn: chondrodite (Lager et al., 2001); Chu: clinohumite (Berry and James, 2001); D: phase D (Nishi et al., 2014); E: phase E (Wang et al., 2022); En: enstatite (Sanchez-Valle and Bass, 2010); Fo: forsterite (Hushur et al., 2009); H: phase H (Ohtani et al., 2014); Hy wds: hydrous wadsleyite (C_{H2O} up to 3.3 wt.%) (Kudoh et al., 1996); Hu: humite (Liu et al., 2021); Nrb: norbegite (Camara, 1997); Shy B: supper hydrous phase B (Ohtani et al., 1995); Srp: serpentine (Mookherjee and Stixrude, 2009); 10 Å: 10-Å phase (Rashchenko et al., 2016); Tlc: talc (Stixrude, 2002).

FIGURE 2. Crystal structures of (a) clinohumite (Berry and James, 2001), (b) humite (Liu et al., 2021), (c) chondrodite (Lager et al., 2001), and (d) forsterite (Hushur et al., 2009). Orange: MO_6 octahedra; blue: SiO_4 tetrahedra; orange spheres: O atoms; blue spheres: Si atoms; red spheres: O atoms; white spheres: H atoms. Crystal structures were drawn using VESTA software (Momma and Izumi, 2011).

FIGURE 3. Representative Brillouin spectra of humite-group minerals at ambient conditions. (a) F-rich clinohumite (F_{45}-Chu); (b) F-poor clinohumite (F_8-Chu); (c) humite (F_{37}-Hu); (d) chondrodite (F_{61}-Chn). Black line: experimental data; colored lines: fitting results. R: Rayleigh line; V_p: quasi-longitudinal acoustic mode; V_{S2}: quasi-transverse fast acoustic mode; V_{S1}: quasi-transversal slow acoustic mode.

FIGURE 4. Measured acoustic velocities of clinohumite. (a)-(c): clinohumite with X_F = 0.45 (F_{45}-Chu); (d)-(f) clinohumite with X_F =0.08 (F_8-Chu), respectively. The orientation of each sample platelet is shown in each panel. Red: V_P; Blue: V_{S2}; Orange: V_{S1}.

FIGURE 5. Measured acoustic velocities of humite and chondrodite. (a)-(c): humite with X_F = 0.37 (F_{37}-Hu); (d)-(f): chondrodite with X_F = 0.61 (F_{61}-Chn), respectively. The orientation of each sample platelet is shown in each panel. Red: V_P; Blue: V_{S2}; Orange: V_{S1}.

FIGURE 6. Elasticity and sound velocities of the humite-group minerals at ambient conditions. (a) elastic modulus as a function of fluorine concentration; (b) elastic modulus as a function of water content; (c) velocity as a function of water content. The solid lines represent the linear fits of the elasticity (sound velocity) for humite-group minerals with less than 1.1 mol% Fe, while the dashed line is obtained by assuming a linear reduction in the elasticity (sound velocity) caused by the presence of Fe at a given H_2O content. Red solid circles: clinohumite in this study; red open circles: clinohumite from previous studies (Fritzel and Bass, 1997; Phan, 2008); orange triangles: humite in this study; blue solid circles: chondrodite in this study; blue open circles: chondrodite from previous studies (Sinogeikin and Bass, 1999; Ye et al., 2015).

FIGURE 7. Velocities of major mantle minerals and humite-group minerals at ambient conditions. Blue circles: major mantle minerals, including olivine (Mao et al., 2015), orthopyroxene (Li et al., 2022), clinopyroxene (Li and Neuville, 2010), wadsleyite (Mao et al., 2015), garnet (Wei et al., 2021), phase A (Cai et al., 2021; Sanchez-Valle et al., 2006), and phase E (Satta et al., 2019; Wang et al., 2022). Red circles: the F-bearing humite-group minerals reported in this study, including F_{61}-chondrodite, F_{37}-humite, F_8-clinohumite, and F_{45}-clinohumite. More details can be found in Online Material[1] Table S10.

FIGURE 8. Density, elasticity, and sound velocities of minerals along the forsterite-brucite join at ambient conditions. (a) density, ρ; (b) adiabatic bulk moduli (K_{S0}) and shear moduli (G_0); (c) Compressional- (V_P) and shear-wave velocities (V_S). Red line: the trends for Mg-end member compositions; blue line: the trends for Fe-end member compositions with the same slope as trends for Mg-end members. Circles: olivine; squares: humite-group minerals; diamonds: phase A; triangles: brucite; stars: humite-group minerals of this study. Colors are related to the mole percentage of Fe in these minerals, with red indicating Fe content below 10%, while blue represents the Fe-end member.

FIGURE 9. Elasticity and sound velocities of minerals along the forsterite-brucite join as a function of density. (a) elasticity; (b) sound velocities. Circles: forsterite (olivine); squares: humite-group minerals; diamonds: phase A; triangles: brucite; stars: humite-group minerals of this study. Colors are related to the mole percentage of Fe in these minerals.

798

This is the peer-reviewed, final accepted version for American Mineralogist, published by the Mineralogical Society of America.
The published version is subject to change. Cite as Authors (Year) Title. American Mineralogist, in press.
DOI: https://doi.org/10.2138/am-2023-9067. http://www.minsocam.org/

799
800 **TABLE 1.** Composition of humite-group minerals from electron microprobe analyses [a]
801

Oxide (wt.%)	F_{45}-Chu	F_8-Chu	F_{37}-Hu	F_{61}-Chn
MgO	56.99(45)	55.33(25)	57.49(24)	56.80(22)
FeO	0.09(3)	1.09(7)	0.29(7)	0.17(7)
CaO	--	0.026(6)	0.021(8)	0.026(9)
MnO	0.02(2)	0.05(5)	0.01(2)	0.017(17)
Al_2O_3	0.008(11)	0.02(1)	0.009(11)	0.005(8)
SiO_2	37.75(31)	37.98(20)	37.44(15)	33.60(20)
F	2.71(9)	0.47(25)	2.86(17)	6.70(14)
TiO_2	2.39(8)	3.06(5)	0.42(2)	0.15(2)
H_2O[b]	1.5	2.5	2.2	1.9
Atom (apfu[c])				
Mg	8.85	8.63	7.03	4.88
Fe	0.008	0.10	0.02	0.01
Ca	--	0.003	0.002	0.002
Mn	0.002	0.005	0.001	0.001
Al	0.001	0.003	0.001	0.002
Si	3.93	3.97	3.07	1.94
F	0.89	0.16	0.74	1.22
Ti	0.19	0.24	0.03	0.006

[a] EMPA uses a fixed oxygen atom counting method, converting the weight percentage of oxide into atomic or molecular ratios.
[b] The wt.% of H_2O/H is calculated from stoichiometry, assuming the mole ratio H:O to be 2:18.
[c] Atoms per formula unit, the propagated errors are in the parentheses

802
803
804 **TABLE 2.** The unit-cell parameters and density of humite-group minerals at ambient conditions
805
806

	F_{45}-Chu	F_8-Chu	F_{37}-Hu	F_{61}-Chn
807 a (Å)	13.6423(3)	13.6387(7)	20.8114(13)	7.8284(2)
808 b (Å)	4.7364(1)	4.7333(2)	4.7353(3)	4.7272(1)
809 c (Å)	10.2332(3)	10.2346(5)	10.2421(6)	10.2481(3)
810 β °	100.910(1)	100.918(2)	90	109.140(1)
V (Å^3)	649.27(4)	648.75(8)	1009.34(17)	358.28 (3)
811 ρ (g/cm^3)	3.208(1)	3.219(1)	3.207(1)	3.136(1)

812
813

This is the peer-reviewed, final accepted version for American Mineralogist, published by the Mineralogical Society of America.
The published version is subject to change. Cite as Authors (Year) Title. American Mineralogist, in press.
DOI: https://doi.org/10.2138/am-2023-9067. http://www.minsocam.org/

814

815 **TABLE 3.** Elastic properties of humite-group minerals under ambient conditions

816

	Clinohumite (Chu)			Chondrodite (Chn)			Humite (Hu)
	F_{45}-Chu (This study)	F_8-Chu (This study)	F_{29}-Chu[a]	F_{61}-Chn (This study)	F_{32}-Chn[b]	OH-Chn[c]	F_{37}-Hu (This study)
ρ (g/cm^3)	3.208(1)	3.219(1)	3.261(1)	3.136(1)	3.227(10)	3.099(1)	3.207(1)
C_{ij} (GPa)							
C_{11} (C_{33})	210.6(9)	211.1(7)	212(2)	192.1(9)	213.4(15)	188.0(7)	220.0(17)
C_{22} (C_{11})	314.1(13)	301.7(6)	296(2)	285.2(8)	275.3(15)	278.0(10)	292.5(11)
C_{33} (C_{22})	206.2(9)	194.2(8)	191(2)	198.8(9)	198.4(12)	195.7(7)	200.6(12)
C_{44} (C_{66})	79.3(7)	75.2(5)	72.0(8)	74.5(10)	69.7(6)	64.0(10)	76.5(6)
C_{55} (C_{44})	71.8(4)	66.6(4)	65(1)	70.8(5)	72.1(9)	68.3(4)	70.1(6)
C_{66} (C_{55})	80.1(5)	78.2(3)	74.3(8)	74.5(9)	75.2(7)	71.3(5)	78.2(7)
C_{12} (C_{13})	69.8(9)	67.5(8)	66(3)	65.1(27)	70(3)	61(10)	67.0(27)
C_{13} (C_{23})	72.9(7)	64.2(9)	80(4)	71.3(7)	59(2)	71.4(7)	68.8(14)
C_{23} (C_{12})	69.1(15)	66.3(16)	72(7)	74.7(26)	67(3)	74(3)	64.0(12)
C_{15} (C_{14})	9.3(5)	-11.1(6)	-0.3(6)	0.5(5)	7.2(10)	3.9(4)	
C_{25} (C_{24})	3.9(10)	-0.8(14)	1(2)	-2.1(24)	-1.7(12)	2.6(10)	
C_{35} (C_{34})	5.1(5)	-3.3(5)	2(1)	5.5(6)	-2.6(8)	2.5(4)	
C_{46} (C_{56})	1.6(5)	-0.6(4)	-0.6(7)	0.4(7)	-0.7(4)	4.1(6)	
RMS (m/s)	32	20	94	20	84	39	38
β_a (GPa^{-1})	0.0031(1)	0.0031(1)	0.0029(1)	0.0034(1)	0.0031(1)	0.0035(1)	0.0029(1)
β_b (GPa^{-1})	0.0018(1)	0.0019(1)	0.0019(1)	0.0019(1)	0.0020(1)	0.0020(1)	0.0020(1)
β_c (GPa^{-1})	0.0032(1)	0.0035(1)	0.0033(1)	0.0031(1)	0.0034(1)	0.0031(1)	0.0034(1)
AV_P (%)	23.1	24.2	21.9	19.7	16.7	19.9	18.8
AV_S (%)	15.0	16.2	16.5	14.1	12.3	15.9	12.1
K_{Voigt} (GPa)	128.3(5)	122.6(5)	126.1(19)	122.0(9)	119.9(11)	119.4(23)	123.6(8)
G_{Voigt} (GPa)	80.8(2)	77.9(2)	74.3(6)	75.0(3)	76.1(4)	71.1(7)	79.2(3)
K_{Reuss} (GPa)	124.1(4)	120.5(4)	123.3(35)	118.8(8)	117.4(30)	116.4(16)	121.1(6)
G_{Reuss} (GPa)	78.5(4)	75.7(4)	72(10)	73.3(10)	75.0(14)	69.2(7)	77.6(3)
K_{S0} (GPa)	126.2 (3)	120.5(3)	125(2)	120.4(6)	118.4(16)	118(1)	122.4(5)
G_0 (GPa)	79.7(2)	76.8(2)	73(5)	74.1(5)	75.6(7)	70.6(5)	78.4(2)
V_P (km/s)	8.51(1)	8.32(1)	8.26(9)	8.36(2)	8.24(5)	8.26(8)	8.41(1)
V_S (km/s)	4.98(1)	4.88(1)	4.7(3)	4.86(2)	4.84(3)	4.76(4)	4.94(1)

Notes: The elastic constants are given in the standard monoclinic coordinate system (*b*-unique, $P2_1/c$), while the values inside parentheses are those for an *a*-unique coordinate system ($P2_1/b$).
[a]Fritzel and Bass (1997): $Mg_{8.85}Fe_{0.57}Si_{4.07}O_{16}(OH_{1.41}F_{0.57})$
[b]Sinogeikin and Bass (1999): $Mg_{4.69}Fe_{0.27}Mn_{0.01}Ti_{0.02}(SiO_4)_2F_{0.63}(OH)_{1.33}O_{0.04}$
[c]Ye et al. (2015): $Mg_{5.047}Fe_{0.058}Si_{1.945}O_{10}H_2$

817

This is the peer-reviewed, final accepted version for American Mineralogist, published by the Mineralogical Society of America.
The published version is subject to change. Cite as Authors (Year) Title. American Mineralogist, in press.
DOI: https://doi.org/10.2138/am-2023-9067. http://www.minsocam.org/

818
819 **TABLE 4.** Isotropic aggregate properties of minerals along the forsterite-brucite join
820

Mineral	C_{H_2O} (wt.%)	X_{Fe} (mol%)	ρ (g/cm^3)	K_{S0} (GPa)	G_0 (GPa)	V_P (km/s)	V_S (km/s)
Olivine							
Sumino (1979)	0	100	4.400	137.9(14)	50.9(1)	6.84(3)	3.40(1)
Suzuki et al. (1983)	0	0	3.225(1)	128.9(2)	81.4(2)	8.58(1)	5.02(1)
Webb (1989)	0	9.4	3.348(3)	128.9	81.1	8.42	4.92
Isaak et al. (1989)	0	0	3.222(7)	128.8(5)	81.8(2)	8.59(3)	5.04(5)
Zaug et al. (1993)	0	10	3.340	129.0(6)	77.6(4)	8.33(4)	4.82(2)
Isaak et al. (1993)	0	100	4.387(6)	135.8(13)	50.9(3)	6.82(3)	3.41(1)
Zha et al. (1996)	0	0	3.221(1)	128.8(5)	81.6(2)	8.59(3)	5.03(1)
Abramson et al. (1997)	0	10.8	3.355	129.4(5)	78.0(3)	8.34(4)	4.82(2)
Zha et al. (1998)	0	10	3.343(1)	131.1(19)	79.4(8)	8.42(9)	4.87(5)
Darling et al. (2004)	0	9.4	3.311	127.1(6)	77.5(3)	8.31(4)	4.81(2)
Li et al. (2004)	0	0	3.222(7)	125(5)	81(1)	8.50(5)	5.01(2)
Speziale et al. (2004)	0	94	4.388(9)	137.6 (3)	51.2(2)	6.85(1)	3.42(1)
Liu et al. (2005)	0	10	3.342	130.3(4)	77.4(2)	8.36(5)	4.81(2)
Jacobsen et al. (2008)	0.8	3.0	3.240(3)	125.2(8)	77.7(3)	8.40(1)	4.90(1)
Jacobsen et al. (2008)	0.9	0	3.180(3)	125.4(2)	79.6(1)	8.53(1)	5.00(1)
Wang (2008)	0.6	8	3.292	128.6(11)	79.0(3)	8.43(5)	4.90(1)
Mao et al. (2015)	0	10.0	3.343(3)	129.8(9)	77.8(5)	8.36(1)	4.82(1)
Zhang and Bass (2016)	0	9.5	3.341(3)	129(2)	78(2)	8.33(3)	4.80(3)
Faccincani et al. (2023)	0.2	9.8	3.345(6)	129.5(3)	78.1(1)	8.36(1)	4.83(1)
Clinohumite							
Fritzel and Bass (1997)	2.0	6.1	3.261(1)	125(2)	73(5)	8.26(9)	4.7(3)
Phan (2008)	2.9	0	3.134(1)	119(2)	77(1)	8.41(9)	4.96(8)
Zhang et al. (2023)	1.7	0	3.199(2)	121.0(5)	76.5(2)	8.40(2)	4.90(2)
F_{45}-Chu_{98}, this study	1.6	0	3.208(1)	126.2(3)	79.7(2)	8.51(1)	4.98(1)
F_8-Chu_{96}, this study	2.6	1.1	3.219(1)	120.5(3)	76.8(2)	8.32(1)	4.88(1)
Humite							
F_{37}-Hu_{100}, this study	2.4	0	3.207(1)	122.4(3)	78.4(2)	8.41(1)	4.94(1)
Chondrodite							
Sinogeikin and Bass (1999)	3.3	5.4	3.227(10)	118.4(16)	75.6(7)	8.24(5)	4.84(3)
Ye et al. (2015)	5.3	1.1	3.099(1)	117.9(12)	70.1(5)	8.26(8)	4.76(4)
F_{61}-Chn_{100}, this study	2.1	0	3.136(1)	120.4(3)	74.1(5)	8.36(2)	4.86(2)
Phase A							
Sanchez-Valle et al. (2006)	11.7	1.9	2.976(1)	106(1)	61(1)	7.93(8)	4.53(8)
Phan (2008)	11.8	0	2.949(1)	100(2)	61(1)	7.84(9)	4.55(8)
Cai et al. (2021)	11.8	0	2.973(2)	102.1(5)	66.7(3)	8.02(1)	4.74(1)
Brucite							
Xia et al. (1998)	30.9	0	2.380(1)	46(1)	34.9(5)	6.2(1)	3.83(5)
Jiang et al. (2006)	30.9	0	2.380(1)	43.8(8)	35.2(3)	6.2(1)	3.85(3)

This is the peer-reviewed, final accepted version for American Mineralogist, published by the Mineralogical Society of America.
The published version is subject to change. Cite as Authors (Year) Title. American Mineralogist, in press.
DOI: https://doi.org/10.2138/am-2023-9067. http://www.minsocam.org/

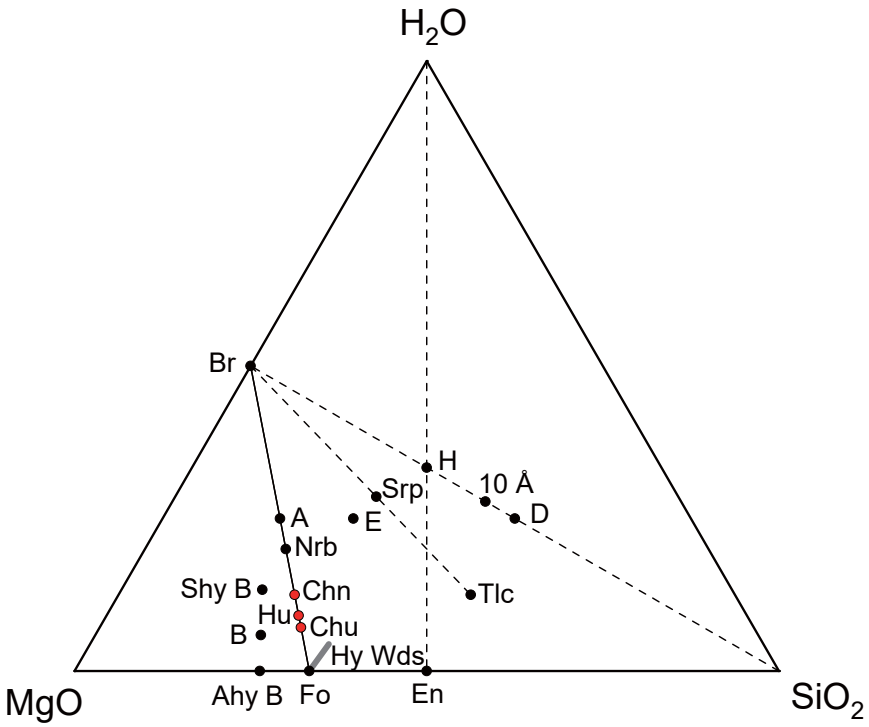

Figure 1

This is the peer-reviewed, final accepted version for American Mineralogist, published by the Mineralogical Society of America.
The published version is subject to change. Cite as Authors (Year) Title. American Mineralogist, in press.
DOI: https://doi.org/10.2138/am-2023-9067. http://www.minsocam.org/

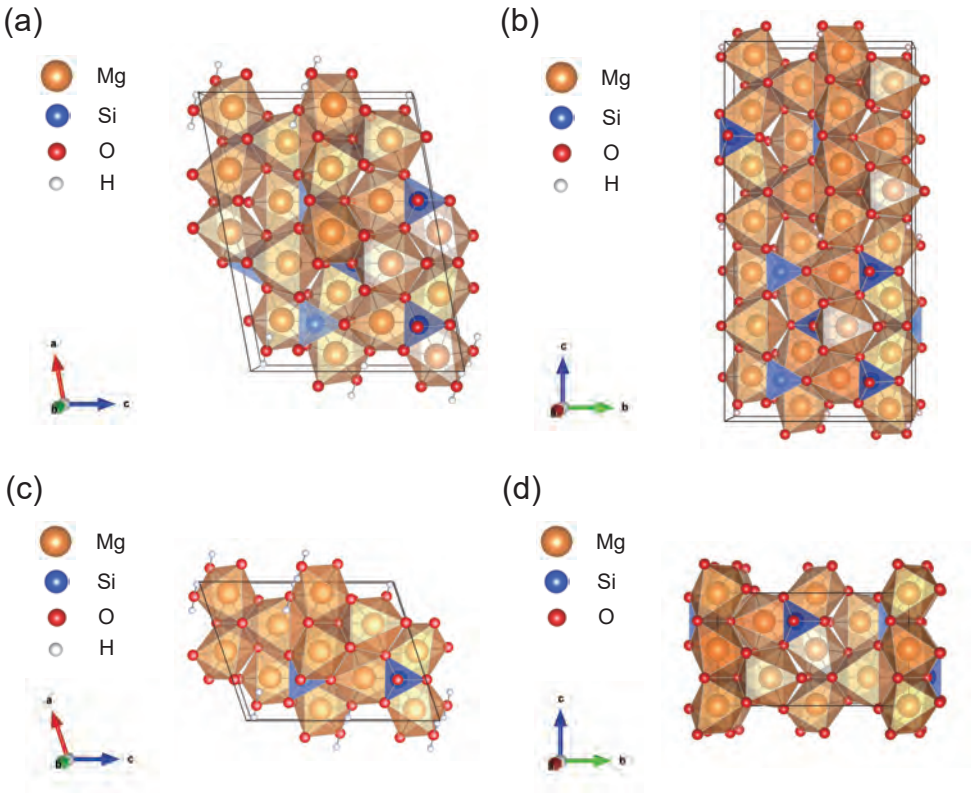

Figure 2

This is the peer-reviewed, final accepted version for American Mineralogist, published by the Mineralogical Society of America.
The published version is subject to change. Cite as Authors (Year) Title. American Mineralogist, in press.
DOI: https://doi.org/10.2138/am-2023-9067. http://www.minsocam.org/

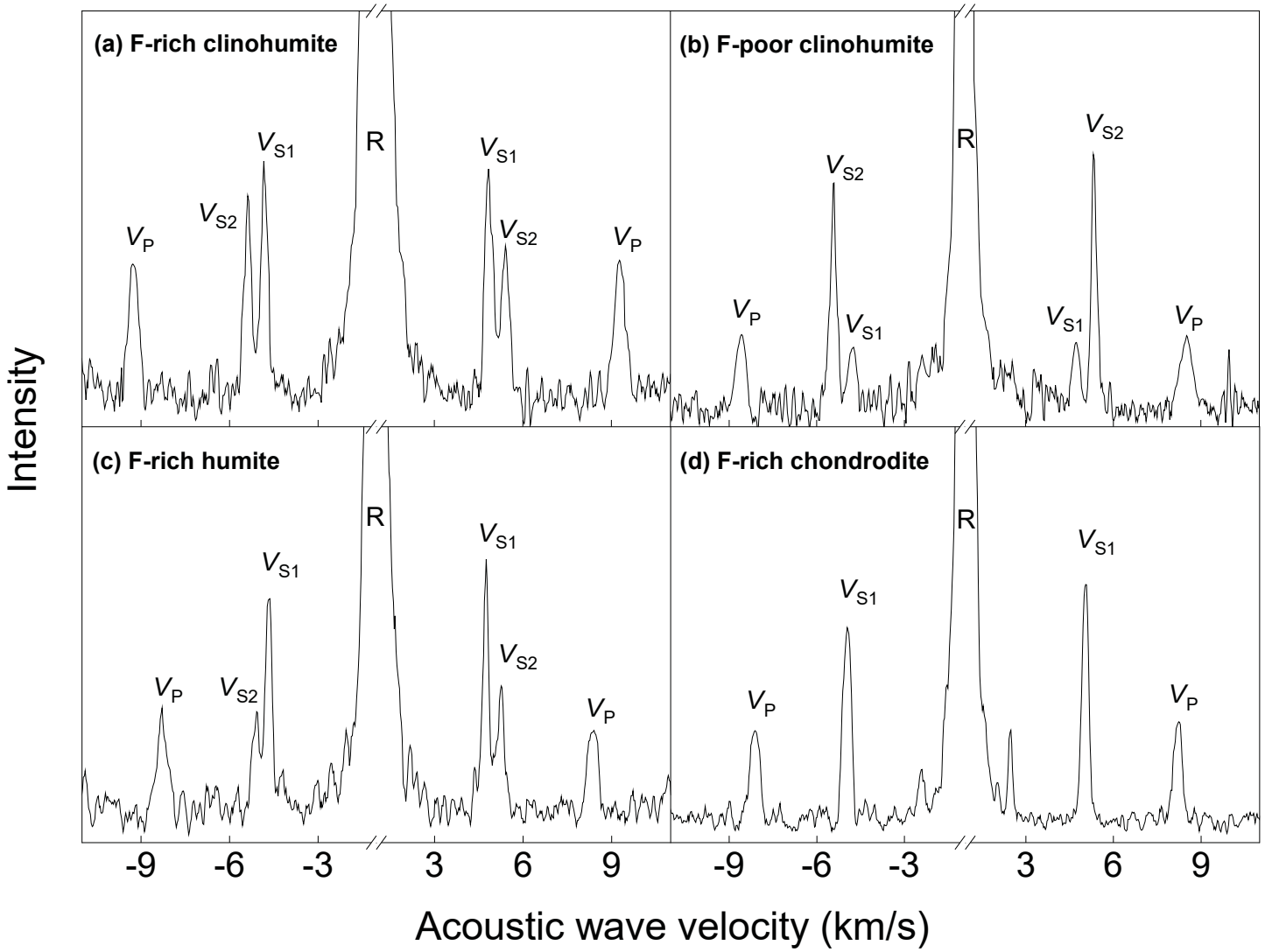

Figure 3

This is the peer-reviewed, final accepted version for American Mineralogist, published by the Mineralogical Society of America.
The published version is subject to change. Cite as Authors (Year) Title. American Mineralogist, in press.
DOI: https://doi.org/10.2138/am-2023-9067. http://www.minsocam.org/

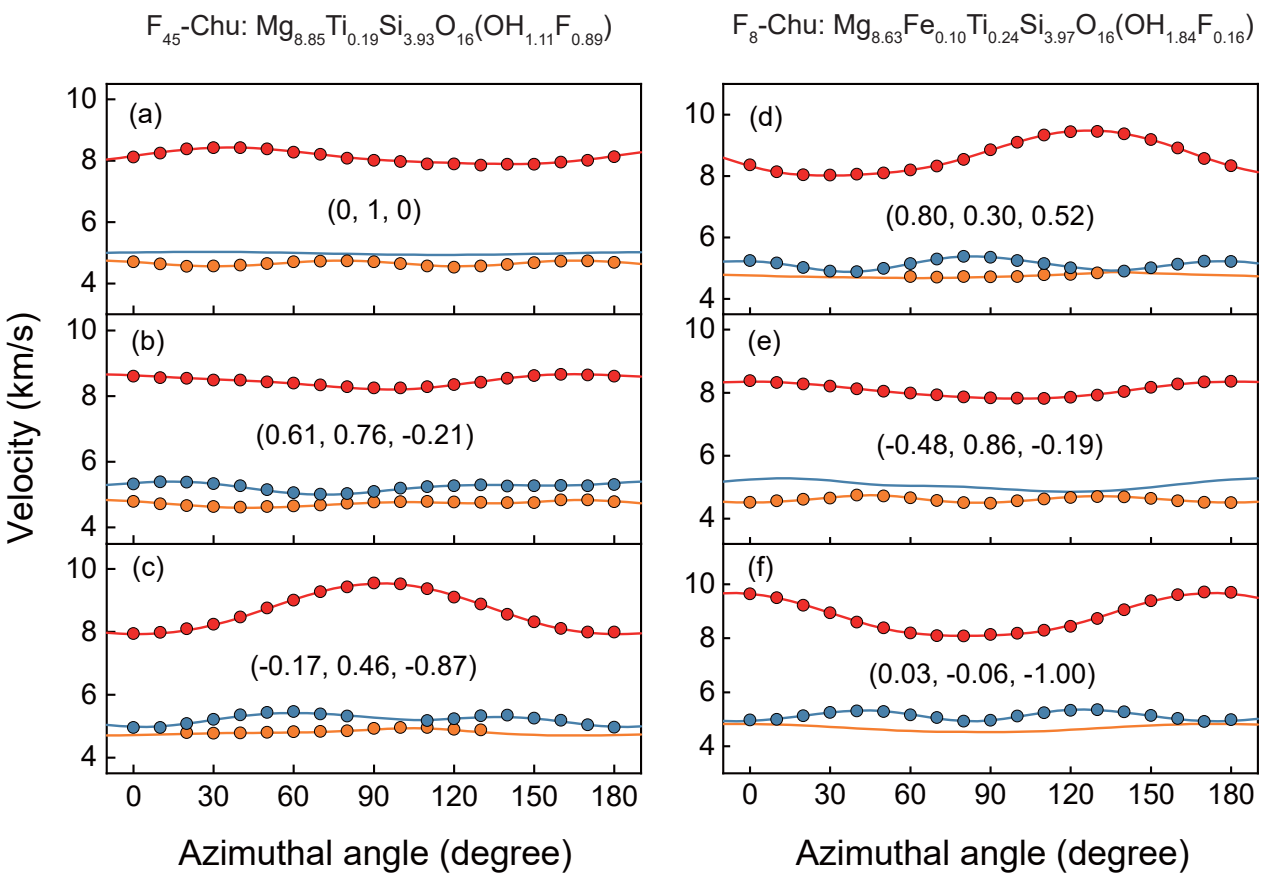

Figure 4

This is the peer-reviewed, final accepted version for American Mineralogist, published by the Mineralogical Society of America.
The published version is subject to change. Cite as Authors (Year) Title. American Mineralogist, in press.
DOI: https://doi.org/10.2138/am-2023-9067. http://www.minsocam.org/

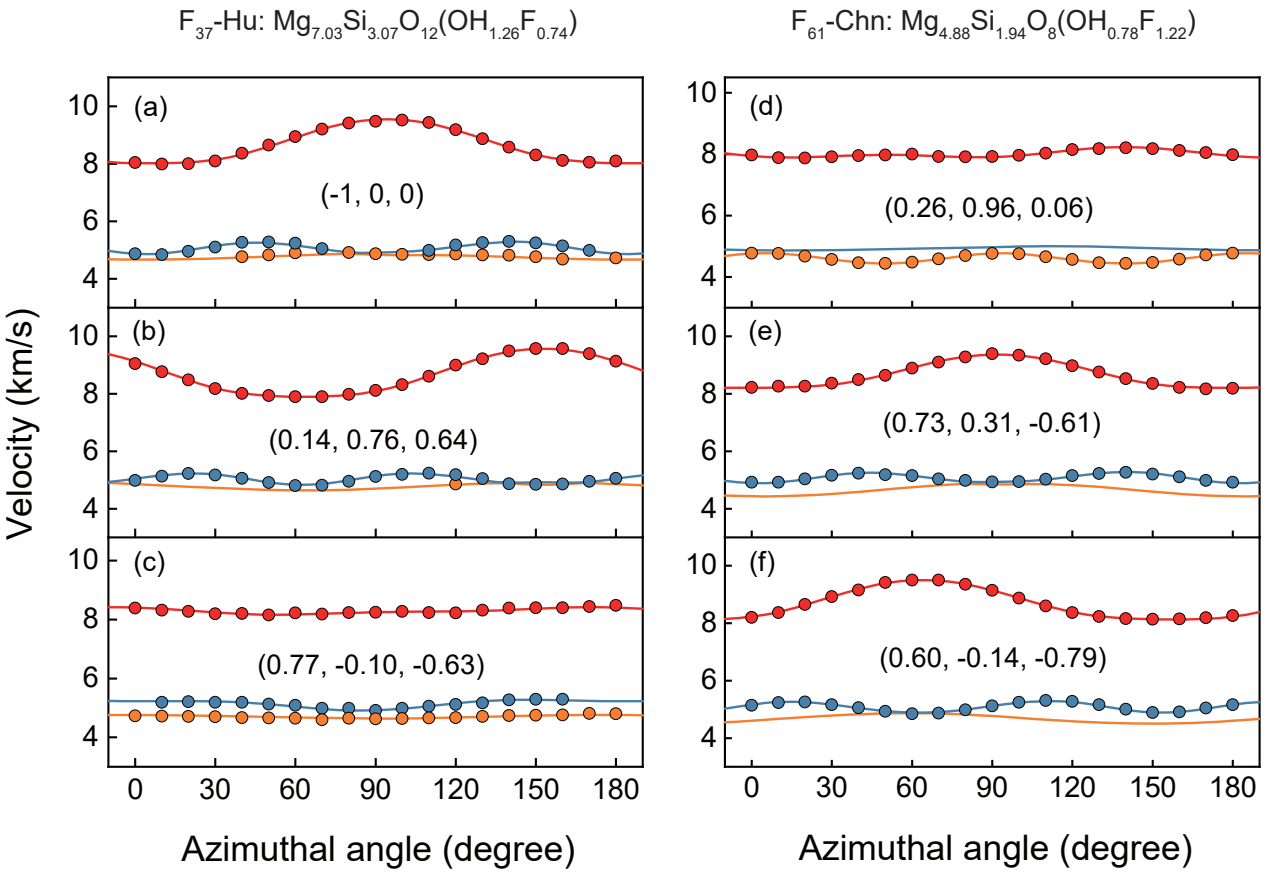

Figure 5

This is the peer-reviewed, final accepted version for American Mineralogist, published by the Mineralogical Society of America.
The published version is subject to change. Cite as Authors (Year) Title. American Mineralogist, in press.
DOI: https://doi.org/10.2138/am-2023-9067. http://www.minsocam.org/

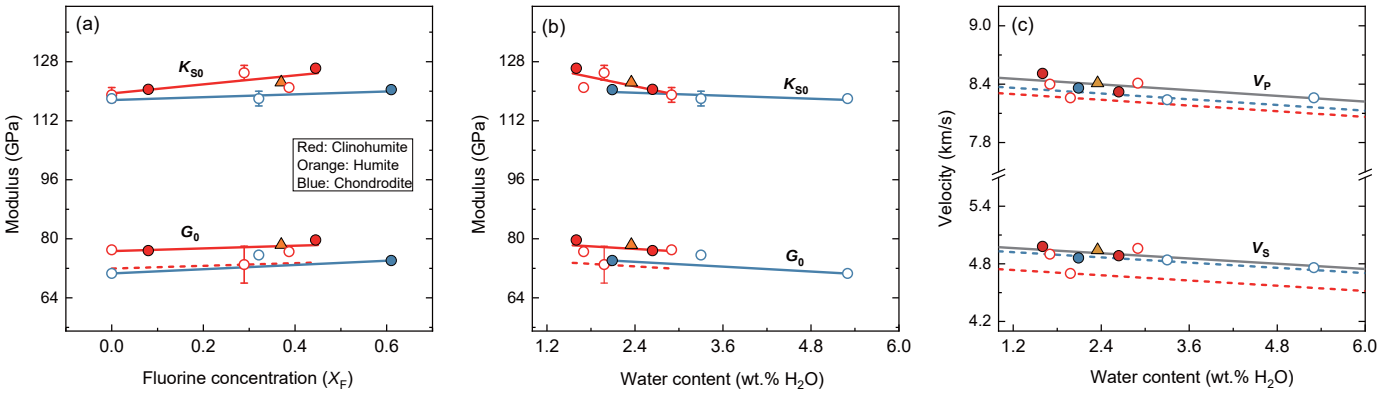

Figure 6

This is the peer-reviewed, final accepted version for American Mineralogist, published by the Mineralogical Society of America.
The published version is subject to change. Cite as Authors (Year) Title. American Mineralogist, in press.
DOI: https://doi.org/10.2138/am-2023-9067. http://www.minsocam.org/

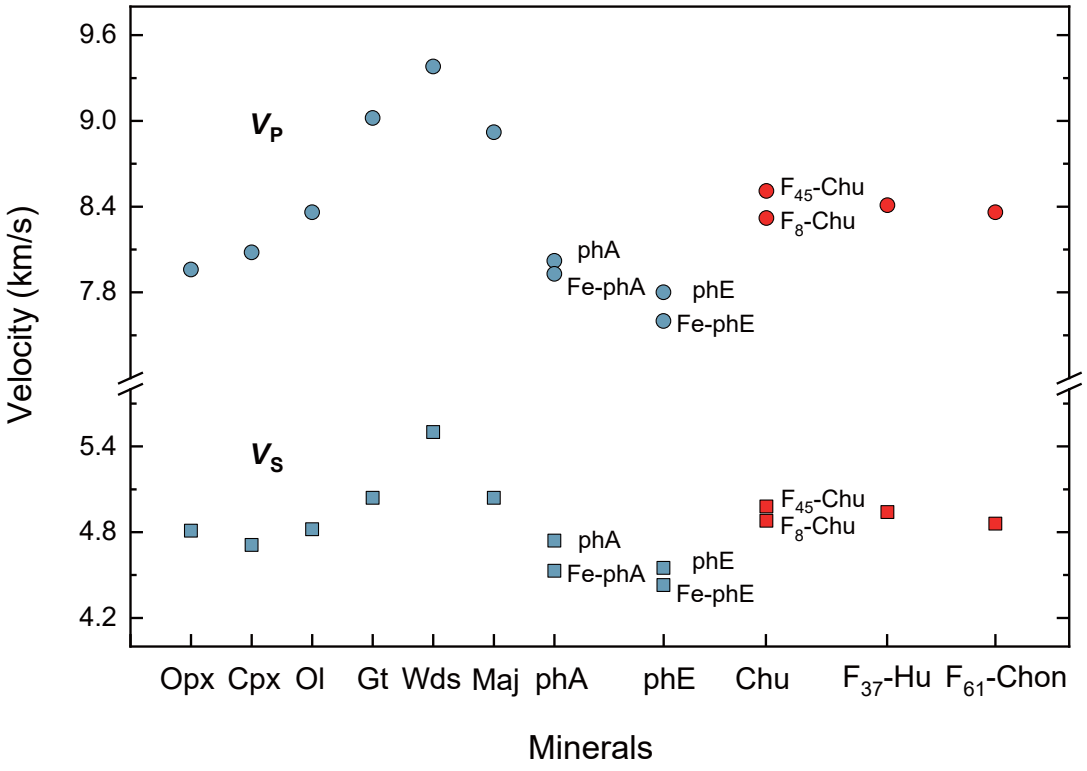

Figure 7

This is the peer-reviewed, final accepted version for American Mineralogist, published by the Mineralogical Society of America.
The published version is subject to change. Cite as Authors (Year) Title. American Mineralogist, in press.
DOI: https://doi.org/10.2138/am-2023-9067. http://www.minsocam.org/

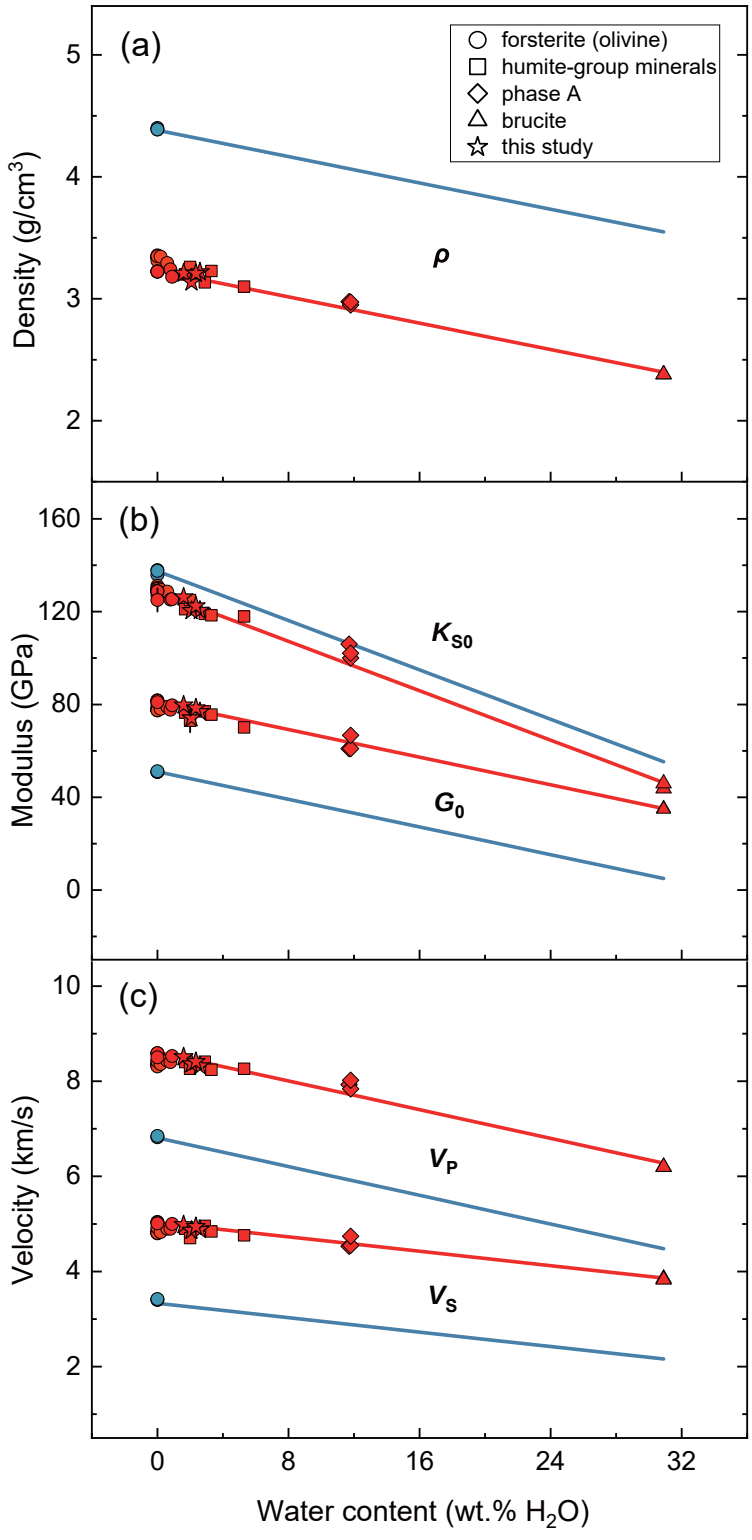

Figure 8

This is the peer-reviewed, final accepted version for American Mineralogist, published by the Mineralogical Society of America.
The published version is subject to change. Cite as Authors (Year) Title. American Mineralogist, in press.
DOI: https://doi.org/10.2138/am-2023-9067. http://www.minsocam.org/

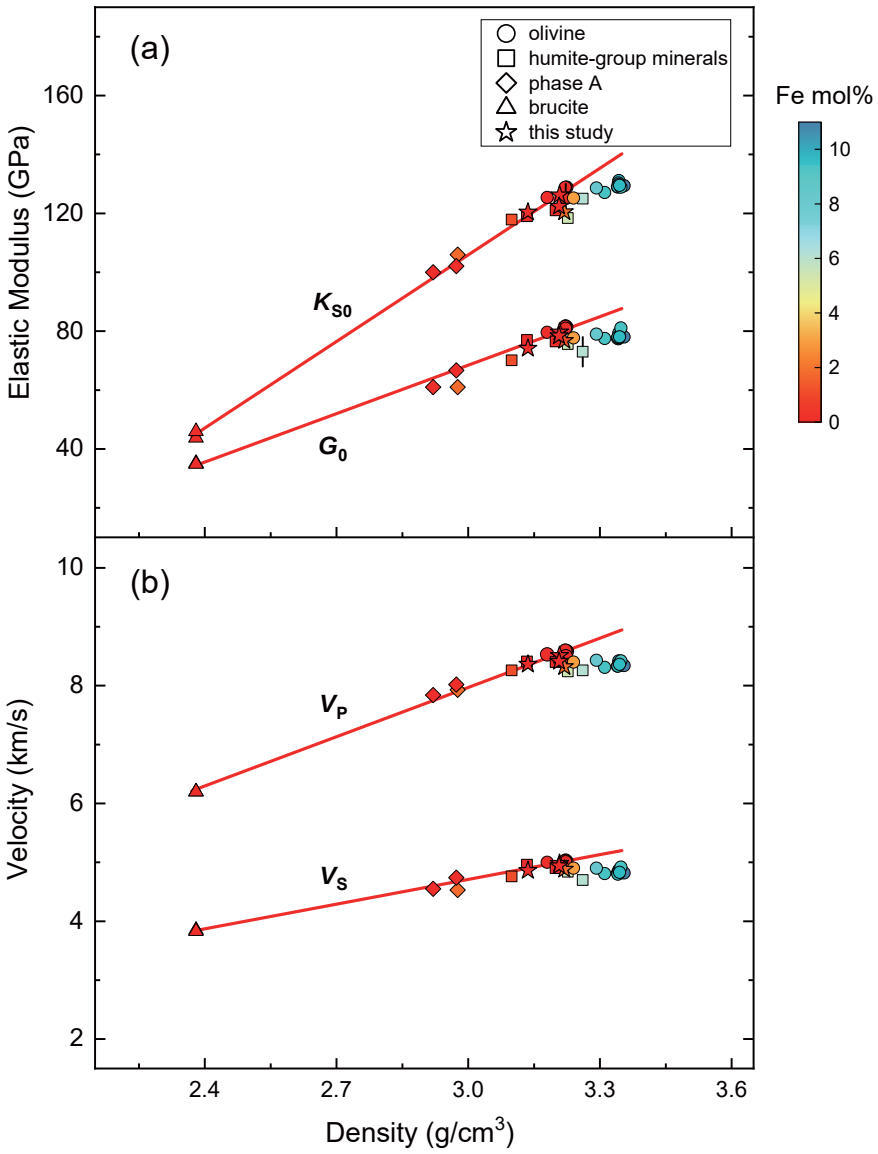

Figure 9